2018

Development and Implementation of an Ultrasonic Method to Characterize Acoustic and Mechanical Fingernail Properties

Rares Anthony Vacarescu
University of Windsor

Development and Implementation of an Ultrasonic Method to Characterize Acoustic and Mechanical Fingernail Properties

By

Rares Anthony Vacarescu

A Thesis
Submitted to the Faculty of Graduate Studies
through the Department of Physics
in Partial Fulfillment of the Requirements for
the Degree of Master of Science
at the University of Windsor

Windsor, Ontario, Canada

2018

Development and Implementation of an Ultrasonic Method to Characterize Acoustic and Mechanical Fingernail Properties

By

Rares Anthony Vacarescu

APPROVED BY:

_____

H. Zhang
Department of Biological Science

_____

D. Xiao
Department of Physics

_____

R. Gr. Maev, Advisor
Department of Physics

December 15, 2017

DECLARATION OF CO-AUTHORSHIP / PREVIOUS PUBLICATION

I. Co-Authorship Declaration

I hereby declare that this thesis incorporates material that is result of joint research, as follows: Chapter 2 of the thesis was co-authored with Bartosz Slak under the supervision of professor Roman Maev. In all cases, the main ideas, primary contributions, experimental designs, data analysis, interpretation, and writing were performed by the author, and the contribution of co-authors was primarily through provision of literature review and text editing. Natalie Lewoc and Andrew Daabous contributed to some literature review text; Anna Maeva and Emil Strumban contributed by providing refinement and editing of the manuscript; Caroline Hamm contributed by providing the necessary patients for the data collection at the hospital; Bartosz Slak and Roman Maev contributed by providing supervision of the project and editing throughout the manuscript.

I am aware of the University of Windsor Senate Policy on Authorship and I certify that I have properly acknowledged the contribution of other researchers to my thesis, and have obtained written permission from each of the co-author(s) to include the above material(s) in my thesis.

I certify that, with the above qualification, this thesis, and the research to which it refers, is the product of my own work.

II. Declaration of Previous Publication

This thesis includes materials from 2 original papers that have been previously published/submitted for publication in peer reviewed journals, as follows:

Thesis Chapter	Publication title/ full citation	Publication Status
Chapter 2	R. Vacarescu, B. Slak, A. Maeva, C. Hamm, N. Lewoc, A. Daabous, E. Strumban and R. Maev, "Investigation of a correlation between taxane-based chemotherapy and the ultrasonic time-of-flight of human fingernails," *Skin Research & Technology,* pp. 1-6, 2017.	*"Published"*

Chapter 2	R. A. Vacarescu, B. Slak, A. Maeva and R. G. Maev, "Portable high-frequency device for cosmetic and clinical fingernail assessment," *2017 IEEE 30th Canadian Conference on Electrical and Computer Engineering (CCECE)*, Windsor, ON, 2017, pp. 1-4. doi: 10.1109/CCECE.2017.7946591	*"Published"*

I certify that I have obtained a written permission from the copyright owners to include the above published materials in my thesis. I certify that the above material describes work completed during my registration as graduate student at the University of Windsor.

I declare that, to the best of my knowledge, my thesis does not infringe upon anyone's copyright nor violate any proprietary rights and that any ideas, techniques, quotations, or any other material from the work of other people included in my thesis, published or otherwise, are fully acknowledged in accordance with the standard referencing practices. Furthermore, to the extent that I have included copyrighted material that surpasses the bounds of fair dealing within the meaning of the Canada Copyright Act, I certify that I have obtained a written permission from the copyright owners to include such materials in my thesis.

I declare that this is a true copy of my thesis, including any final revisions, as approved by my thesis committee and the Graduate Studies office, and that this thesis has not been submitted for a higher degree to any other University or Institution.

ABSTRACT

The human fingernail is a vital organ used by humans on a daily basis and can provide an immense supply of information based on the biological feedback of the body. By studying the quantitative mechanical and acoustic properties of fingernails, a better understanding of the scarcely-investigated field of ungual research can be explored. Investigating fingernail properties with the use of pulse-echo ultrasound is the aim of this thesis. This thesis involves the application of a developed portable ultrasonic device in a hospital-based data collection and the advancement of ultrasonic methodology to include the calculation of acoustic impedance, density and elasticity. The results of the thesis show that the reflectance method can be utilized to determine fingernail properties with a maximum 17% deviation from literature. Repeatability of measurements fell within a 95% confidence interval. Thus, the ultrasonic reflectance method was validated and may have potential clinical and cosmetic applications.

DEDICATION

I dedicate this thesis to my parents

ACKNOWLEDGEMENTS

I would first like to gratefully acknowledge my parents Ioana Vacarescu and Lucian Vacarescu for their ongoing support in my academic involvement and their daily sacrifices to ensure my success in life. I would like to express thanks to all members of the University of Windsor for their guidance and assistance throughout my undergraduate and graduate studies; in particular to Dr. Steven Rehse and Mrs. Kimberly Lefebvre from the Department of Physics. Lastly, I owe an enormous debt of gratitude to all previous and current members of the Institute for Diagnostic Imaging Research who have overseen my growth into the student I am today. Special gratitude goes to my principal advisor Dr. Roman Maev who believed in me when no one else would and also to Bartosz Slak, Dr. Eugene Malyarenko, Dr. Fedar Seviaryn, Dr. Ina Seviaryna, Dr. Emil Strumban, Dr, Mircea Pantea, Sabina Baroaniciu, Suong Mancini and Sarah Beneteau who have journeyed with me to completing my academic goals and provided me with the tools and wisdom to reach my full potential. I wish you all the best.

TABLE OF CONTENTS

LIST OF TABLES

LIST OF FIGURES

LIST OF ABBREVIATIONS

FDA	Food and Drug Administration
TOF	Time-of-Flight
SPL	Spatial Pulse Length
A-scan/ A-mode	Amplitude Scan
B-scan/ B-mode	Brightness Scan
M-scan	Motion Scan
CT	Computed Tomography
MRI	Magnetic Resonance Imaging
AC	Adriamycin and Cyclophosphamide
FWHM	Full Width Half Maximum
a.u.	Arbitrary Units
PVDF	Polyvinylidene Flouride
NCI CTC v.3	National Cancer Institute Common Toxicity Criteria Version 3
USB	Universal Serial Bus
FPGA	Field Programmable Gate Array
ADC	Analog to Digital Converter
Avg	Average
AL	Aluminum
CU	Copper
ZI	Zinc

LIST OF SYMBOLS

λ	Wavelength [m]
d	Diameter [m]
P	Pressure [Pa]
V	Volume [cm^3]
n	Number of mols [mol]
R	Ideal Gas Constant [8.3145 m^3 Pa mol^{-1} K^{-1}]
T	Temperature [^oC]
ρ	Density [g/cm^3]
B	Bulk Modulus [Pa]
s	Condensation
t	Time [s]
x	Location in Space [m]
u	Flow Velocity of a fluid [m/s]
c	Speed of Light [$3x10^8$ m/s]
k	Wavenumber [m^{-1}]
x	Displacement [m]
r	Radial Distance [m]
θ	Polar Angle [degrees]
φ	Azimuthal Angle [degrees]
v	Sound Speed [m/s]
Z	Acoustic Impedance [Rayl]
R	Reflectance
T	Transmittance
A_x	Amplitude
I	Intensity [W/m^2]
T	Period [s^{-1}]
α	Attenuation Coefficient [m^{-1}]
E	Elasticity [Pa]
F	Force [N]

L	Length [m]
A	Area [m^2]
σ	Poisson's Ratio
C_L/ C_S/ C_R	Longitudinal, Shear and Rayleigh Sound Speed [m/s]
f	Frequency [Hz]
M	Male
Y	Young's Modulus [Pa]
F_x	Amplitude in frequency domain
V(z)	Voltage as a function of vertical displacement

Chapter 1 INTRODUCTION

Summary: This chapter aims to introduce the motivation of the thesis in terms of why fingernails and ultrasound were used, then to provide background information on the Physics of ultrasound.

1.1 General Introduction and Motivation

Minimal research has been provided in the last three decades in regards to fingernail properties other than mineral testing. This thesis looks to provide greater insight into the mechanical and acoustical properties of human fingernails [1, 2, 3, 4, 5, 6, 7, 8, 9, 10]. Fingernails are important not only for cosmetic purposes but also from a medical perspective, since their properties are highly indicative of the chemical composition of the bloodstream. Therefore, even slight deviations from homeostatic equilibrium would likely manifest in the fingernails as discoloration, texture change and discomfort or pain. Such examples include fingernail deformities brought on by chemotherapy treatment of cancer which can lead to both color and morphological changes [11, 12, 13]. The motivation for this thesis is to provide a novel method of investigating fingernails as biomarkers to possibly diagnose and monitor blood stream variations stemmed from changes in the body alongside current methods. This is to be accomplished by quantitatively assessing human fingernail properties through the use of ultrasound.

This thesis first encompasses a clinical data collection using an ultrasonic prototype device for quantitative measurements of fingernails as a proof-of-concept. Following the data collection, a new procedure to further calculate mechanical properties with an improved ultrasonic probe was established. The data collection was based on the investigation of fingernail time-of-flight (TOF), while the latter method focused on parameters such as acoustic impedance, density and elasticity. Calibrations of the new

device, as well as its resolution characteristics were reviewed. Phantoms with known properties were implemented for calibration and accuracy assessment.

1.2 Fingernail Anatomy and Current Methods of Fingernail Assessment

1.2.1 Fingernails as Possible Biomarkers

Due to their rapid rates of cellular growth and proliferation, fingernails readily provide a means of detecting changes to the chemical composition of the bloodstream [14, 15, 16]. It is well-known that the individual's health status, in addition to environmental factors such as nutrition, temperature and humidity, all play roles in determining the morphologic structure of the fingernails [13, 17]. Their potential for use as biomarkers in diagnosing systemic pathologies stretches back many centuries, and is still in practice today among medically certified personnel in the field of dermatology [13, 18]. In recent decades, there have been several studies dedicated to correlating fingernail properties with underlying disease or chemical elements present in the human body as outlined in Table 1.1. Most of the methods in literature involve the categorization of specific minerals or compounds in fingernails that can either benefit or cause harm to the fingernails, such as keratin or arsenic, respectively. Various methodologies were implemented such as mass spectroscopy and centrifugation; however these *in-vitro* techniques may be somewhat limited in their applicability to a living organism. The fingernails are so easily affected by chemical changes present in the body that there is much promise to further investigate them as biomarkers.

Table 1.1: List of substances in the body that have been investigated by means of fingernails.

Fingernail Biomarker	Reference
Metal Exposure	[1] [2]
Alcohol	[3] [4]
Fluoride	[5] [6]
Arsenic	[7] [8]
Mercury	[8] [9]
Uric Acid	[10] [19]
Keratin	[20] [21]
Cortisol	[22] [23]

1.2.2 Fingernail Anatomy [24]

The anatomical representation of the fingernail and its essential components are illustrated in Fig 1.1.The human fingernail is comprised of a stiff nail plate, soft and hardened tissues inside and around the nail plate, vasculature and nerves. Ventral to the nail plate is the cellular matrix that is responsible for the formation of the nail itself. This tissue contains the main supply of keratinocytes required for the advancement of nail growth. The other main subungual component of the nail is the nail bed. The matrix and nail bed are in contact with each other but have slightly different characteristics and roles. While the matrix is mainly closest to the proximal portion of the nail (15-25% of the tissue) and extends distally to form the eponychium (cuticle). The remaining 75-85% of tissue is the nail bed which spreads distally to the hyponychium (fingertip). Dorsal to the nail matrix on the visible surface of the finger located proximally is the proximal nail fold, which forms even before the fingernail plate emerges, acting as a barrier to repel and protect against external bacteria and damage to the matrix. Attached to all of these described tissues is the fundamental nail plate formed from a class of stratum corneum giving rise to a glossy, hardened and keratinized nail. The nail plate grows distally outwards at a rate of approximately 115 μm per day from the proximal nail fold, lying atop of the matrix and nail bed. Nevertheless, the rate of growth varies greatly between individuals due to countless factors including age, gender, race, diet and outdoor

environment. The remainder of the finger is surrounded by a soft pulp to act as a cushion for the nerves and vasculature when pressure is applied during normal human activity. Blood to the phalanges is supplied from the radial and ulnar arteries, and is drained via the dorsal and palmar veins [25].

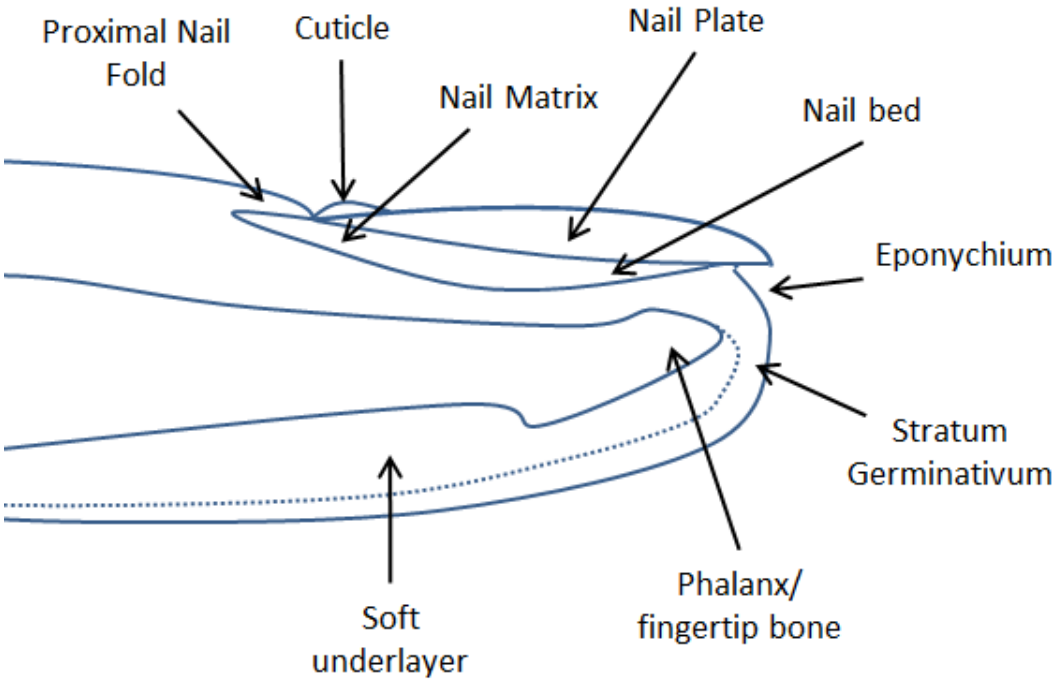

Figure 1.1: Anatomy of the basic components making up the distal portion of the finger in connection with the fingernail.

1.2.3 Comparison of Quantitative Measurement Methods and Ultrasound Literature Review

Numerous methods exist to quantify and assess industrial and biological materials. Microscopy and optical coherence tomography (OCT) involves capturing a zoomed-in, high resolution, digital image. This method provides a visual, qualitative perspective of the color and texture of the fingernail which are altered depending on the lighting, saturations and other discrepancies; minimal quantitative information about the internal structure can be obtained [26]. Similarly, making use of a micrometer to measure changes in the distal edge of the nail plate is not an exact representation of the entire nail thickness and has appreciable error due to the device's precision and the skill of the user.

Spectroscopy identifies which molecules are present in the fingernail based on the intensity of light reflected at certain wavelengths and their triggered frequencies. This method was shown to have difficulty distinguishing differences between samples, due to the fact that molecular composition varies between each person [26]. The utilization of x-rays to view the internal structure of the finger is only effective for discerning larger and thicker samples such as bones with higher attenuation; the image obtained from an x-ray film of fingernails is blurry and illegible. In addition, x-ray radiation may induce harmful changes to the body [26]. The final method, magnetic resonance imaging (MRI), provides enhanced detail in structure but not be ideal for fingernails, which possess a low concentration of water. Staining fingernails would be very beneficial for this approach but not a viable option for *in-vivo* study [26]. Contrary to the above methods, ultrasound provides quantitative and qualitative data from A-scans, B-scans and C-scans. It has the ability to non-invasively extract data from in-vivo subjects and causes minimal irradiation to tissues [27]. Also, its depth penetration and resolution can be interchanged depending on the frequency of the transducer [27].

The application of ultrasound in A-mode to explore fingernails was first investigated *in-vivo* by Finlay in 1987, and soon after by Jemec in 1989 [28, 29]. There have since been studies by Maeva, Wollina and Hirai involving B-mode ultrasound but limited data and trials have been performed in regards to a more in-depth quantitative understanding of fingernails [30, 31, 32]. Different methods have been explored including postmortem, *in-vitro* and low-frequency ultrasound analysis [17, 28, 29]. Earlier studies using ultrasound for both quantitative and qualitative assessment have been performed by Jemec, Finlay, Hirai and Wollina with frequencies 16 MHz, 20 MHz, 30MHz and 50 MHz [17, 28, 29, 30, 31, 32]. The target of the study by Jemec et al. was to calculate the speed of sound in fingernails using A-mode ultrasound to determine TOF and a micrometer to measure fingernail thickness of postmortem samples [29]. The articles by Finlay et al. aim to also determine the sound speed in healthy dry versus hydrated fingernails *in-vivo* using similar techniques for measurement [17, 28]. Hirai et al. sought to image the fingernail in B-mode ultrasound *in-vivo* deformities [32]. In contrast to previous studies, Wollina et al. determined nail plate and nail matrix volumes in healthy patients compared to those with diseases of the integumentary system [31].

Lastly, a study by Maeva et al. was performed *in-vivo* on healthy volunteers to image the layers of the fingernail using B-mode ultrasound [30]. With regards to ultrasound, very little quantitative research has been performed on fingernails, and so further investigation is open to discovery.

1.3 General Concepts of Ultrasound

Ultrasonic is the term given to sound waves of frequencies higher than those which can be perceived by humans. These waves are characterized by a frequency above 20,000 Hz. Sonic waves, or audible sound, ranges from 20 – 20,000 Hz, and subsonic waves are below 20 Hz frequency [26]. Ultrasound is characterized by a propagating acoustic or pressure wave, able to transfer mechanical energy while travelling to and from media. An incident acoustic wave strikes a medium interface, and then is partially reflected and partially transmitted. Reflection from different interfaces over a period of time can be recorded, and the time lag between signal receptions used to calculate TOF. A transducer is the term given to a device that converts ultrasonic pulses to digital signals, and vice versa. Two modalities in which ultrasonic signals can be sent and received will be discussed later on.

The applications of ultrasound in both the medical and industrial field are very useful due to the fact that it is non-invasive, non-radiating, relatively inexpensive and it provides very good temporal resolution [26]. Ultrasound is essentially harmless on the basis that it is not used at high intensities for long exposure times. The Food and Drug Administration (FDA) specifies the permitted acoustic output levels for diagnostic ultrasound safety regulations as follows [33]:

Table 1.2: Ultrasound exposure levels set by the FDA [33].

Application	$Intensity_{spatial\ peak\ temporal\ average}$ (mW/cm^2)	$Intensity_{spatial\ peak\ pulse\ average}$ (mW/cm^2)	Mechanical Index
Peripheral Vessel	720	190	1.9
Cardiac	430	190	1.9
Fetal Imaging, abdominal, intraoperative, pediatric, small organ, neonatal cephalic, adult cephalic	94	190	1.9
Ophthalmic	17	28	0.23

During propagation through a non-uniform medium there may be undesired phenomena such as attenuation, diffraction, dispersion and scattering that may cause waves to distort or deviate from their expected paths. These disturbances will be discussed in the below sections. Variations in density and compressibility of a medium may also cause scattering effects. Interface changes produce scattered reflections upon interaction with ultrasonic waves, but these effects decay exponentially over the wave's displacement. A small particle, or point scatterer, disperses the incident wave in all directions, causing distortion of the reflected signals. Many small inhomogeneities can interfere constructively, causing amplification of the received signal, or destructively, causing cancelling-out of the received signal. For the purpose of this thesis we will consider materials to be isotropic and homogenous to avoid complicated situations arising from such conditions.

1.3.1 Ultrasonic Transducer Design and Operation

Ultrasound waves can be created via a piezoelectric crystal governed by the principle of the piezoelectric effect. This principle states that when an electric field is applied to a piezoelectric material, or crystal, it is displaced or deformed as to create a pressure wave in turn of a frequency [34]. Oppositely, if a pressure wave of definite frequency is incident on the crystal, it deforms and consequently induces an electric field [34]. A computer reads the shift in electric field as a voltage change via electrodes

attached to the crystal, and its signal is processed and displayed [34]. A transducer is the name given to the housing in which the crystal is contained, alongside other components such as a backing and matching layer. As the crystal displaces inside the transducer it creates internal waves which are then reflected back to the crystal from the surrounding housing, manifesting as noise. These internal waves are reflected back into the crystal which are unwanted. In order to reduce the reflections as much as possible, the crystal must operate at maximum amplitude which is satisfied at its fundamental resonant frequency [34]. This corresponds to the crystal having a thickness that is half the wavelength of the emitted wave [34]. A specific material called a backing layer is attached to the back of the crystal, which has an acoustic impedance very different than that of the crystal to encourage reflection of backscattered waves during deformation so they are repelled forwards out of the transducer [35]. The backing layer also acts as a dampener to exponentially attenuate the displacement of the crystal's vibrations, so as for it not to vibrate for very long periods of time, but rather in short bursts [34]. In front of the crystal another layer is present called a matching layer. This functions opposite of the backing layer to transmit as much of the emitted wave as possible through a medium [35]. The matching layer acts to increase the transmittance of the wave into a medium by matching the acoustic impedance of the crystal and material being examined [35]. The thickness of the matching layer is vital because when the thickness is equal to an odd integer of ¼ wavelength of the emitted wave the wave is then efficiently transmitted [34].

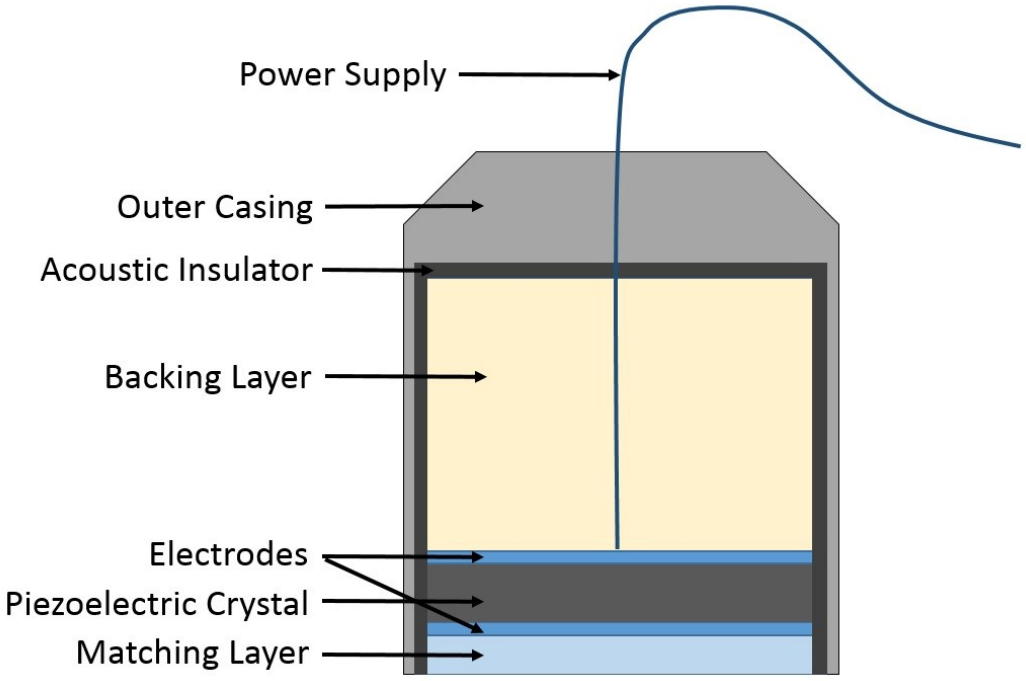

Figure 1.2: Schematic of the internal parts of an ultrasound transducer.

There are two popular modalities of obtaining ultrasonic measurements: pulse-echo mode and through transmission mode. Pulse-echo ultrasound operates on the principle of reflection, whereby a transducer emits a sound wave and 'listens' for a reflected signal back to the same transducer after a brief time delay. This method works best when the interfaces are highly reflective and the subject's anatomy does not feasibly permit the placement of a second transducer. Through transmission operates on the principle of transmission, whereby two transducers are placed on opposing sides of the object to be examined. One transducer emits a sound wave and the other transducer listens for a response wave on the other end. This method works best when reflection and signal are weak from the object. This thesis is based on a transducer operating in pulse-echo mode.

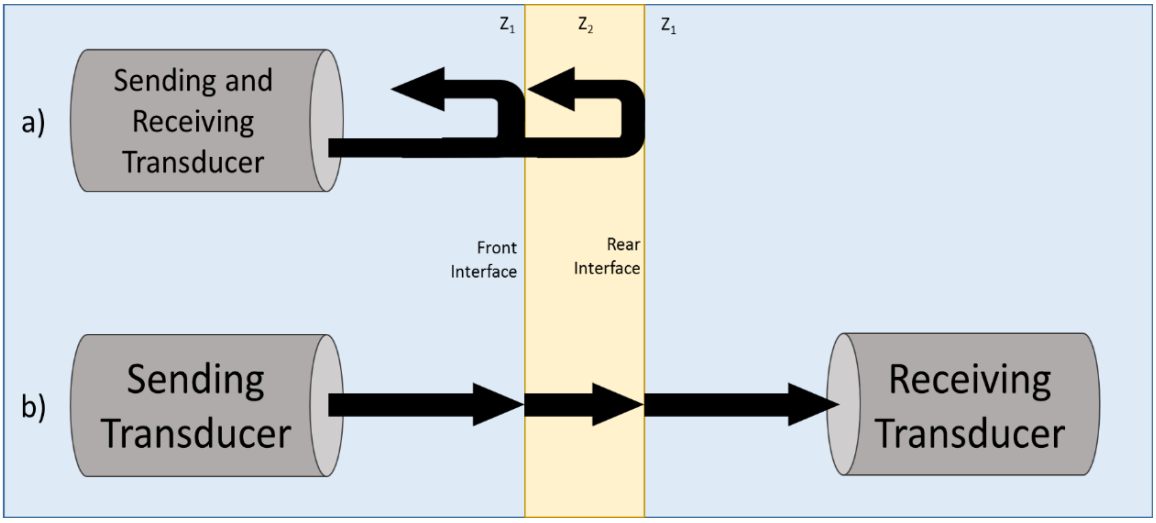

Figure 1.3: Diagram showing a) pulse-echo method and b) though transmission method passing through a boundary of different acoustic impedance than the coupling agent.

1.3.2 Ultrasonic Modes and Resolution [36]

Signals received by the ultrasonic transducer can be acquired in four main modes. These modes have different applications based on the complexity of the sample's shape being measured, changes to the sample in real-time, and the device's scanning capabilities. The four modalities are described below in terms of a single transducer both emitting and receiving ultrasonic signals:

1) Amplitude mode (A-scan)

As an emitted wave is reflected and received back to the transducer, the piezoelectric crystal's displacement is read as a voltage change by electrodes attached to the crystal. The voltage amplitude is recorded as a function of time and presented on a display screen. In A-scans, the transducer is stationary.

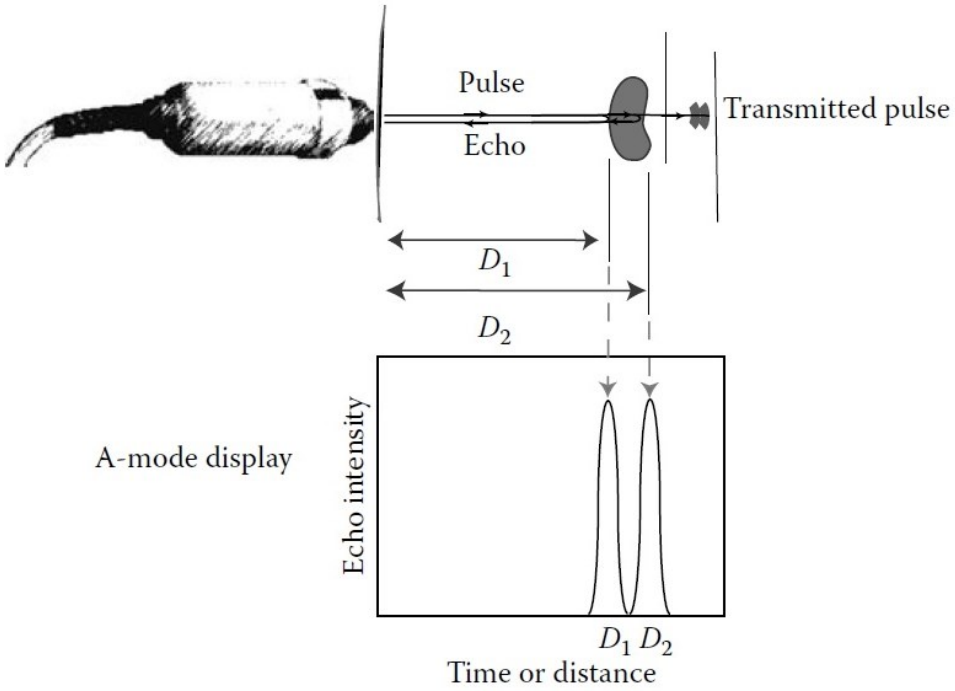

Figure 1.4: Schematic showing on top: a transducer emitting and receiving ultrasonic signal from each interface boundary, and on bottom: the visualization of the A-scan that is seen on a monitor display [26].

2) Brightness mode (B-scan)

As the transducer is translated across the object, it compiles many A-scans for each step of its movement. When these numerous A-scans are combined alongside one another, their values for amplitude can be converted to grayscale to form a two-dimensional image. This image represents the TOF amplitude versus A-scan number. Typically the gray-scale values of the range of amplitudes are subdivided into 256 shades of white to black in an 8-bit system.

3) C-mode (C-scan)

To create a three-dimensional image the transducer can record B-scans as well as an additional translation in the plane perpendicular to that of the B-scan, to form a C-scan. This image represents the TOF amplitude versus A-scan number in one axis versus A-scan number in the remaining third axis.

4) Motion mode (M-scan)

B-scans may be recorded while the object is in motion, yielding a moving image similar to that of a video and called an M-scan. In this mode, the amplitude, signal depth and line number are often displayed along with the moving image.

Ultrasonic frequency is directly proportional to resolution, and inversely proportional to depth of penetration; thus, high-frequency ultrasound is optimal for imaging objects of minimal thickness [37]. There are 3 main resolution labels in an ultrasonic beam: axial, lateral, and elevation resolution. Axial resolution is in the direction of the wave propagation, lateral resolution is perpendicular to that of axial but still in the plane of the propagation, and elevation is in the plane perpendicular to wave propagation [37]. Axial resolution is mathematically expressed as the spatial pulse length or the number of cycles in a pulse (usually 2 or 3) times the wavelength (λ), all divided by two [37]. Another important parameter is spatial pulse length (SPL), which is the distance that a pulse occupies in space, from the start of a pulse to the end of that pulse. It is related to the axial resolution by [37]:

$$Axial\ Resolution = \frac{number\ of\ cycles\ in\ pulse}{2}\lambda = \frac{SPL}{2} \quad (1)$$

The lateral resolution is characterized by the diameter (d) of the pulse wave which is greatest in the area before the focal length. When considering a focused ultrasound beam the lateral resolution at the focal spot is given by the wavelength and radius of transducer (r) [37]:

$$Lateral\ Resolution = \frac{r^2}{\lambda} \quad (2)$$

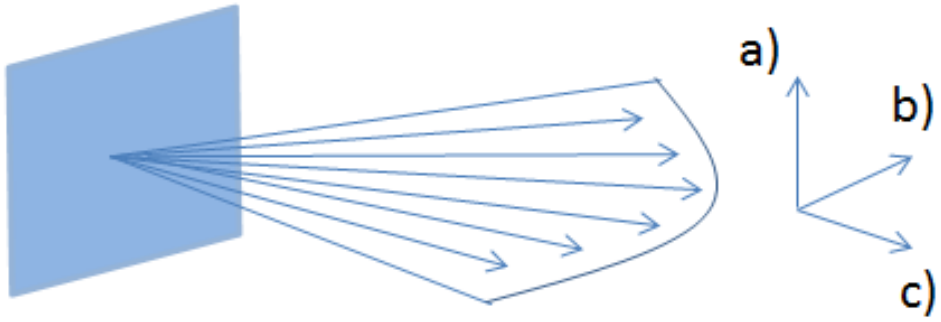

Figure 1.5: Schematic showing the three types of transducer resolution: a) elevation resolution, b) lateral resolution and c) axial resolution.

Lastly, elevation resolution can be related to the beam width similar to lateral resolution. If the aperture at the transducer end is circular, the lateral and elevation resolution are the same; conversely, if the aperture is in any shape other than a circle, the values will be different.

1.3.3 Acoustic Wave Propagation [38]

The study of acoustic waves is governed by the wave equation, which describes a wave propagating through a continuous medium. There are several types of acoustic waves including waves that propagate parallel to the direction of motion (longitudinal waves) and waves that propagate perpendicular to the direction of propagation (transverse or shear waves). Many methods of obtaining and solving the wave equation have been derived, but these derivations put more emphasis on the acoustic derivation of a pressure wave for a fluid. The wave equation in one dimension begins as a linear equation of motion by utilizing the equation of state, the continuity equation, and Euler's force equation.

The ideal gas law starts the derivation by acting as the equation of state:

$$PV = nRT \tag{3}$$

Where P is the pressure, V is the volume, n is the number of mols, R is the ideal gas constant (R = 8.3145 m^3 Pa mol^{-1} K^{-1}) and T is the temperature in Kelvin.

An adiabatic process is considered in which no energy is transferred between the system and its surrounding and so we can express the pressure as a function of a constant expressed as the partial derivative of pressure with respect to density multiplied by the density (ρ):

$$P = \frac{\partial P}{\partial \rho}\rho \tag{4}$$

Separating the pressure and density into components we obtain:

$$P - P_0 = (\frac{\partial P}{\partial \rho})(\rho - \rho_0) \tag{5}$$

The adiabatic bulk modulus (B) for a fluid, the condensation (s) and the acoustic pressure (p) is given by:

$$B = \rho_0(\frac{\partial P}{\partial \rho}) \tag{6}$$

$$s = \frac{\rho - \rho_0}{\rho_0} \tag{7}$$

$$p = P - P_0 \tag{8}$$

Thus, now the pressure can be simply expressed as a linear equation of state as a function of the bulk modulus and the condensation:

$$p = Bs \tag{9}$$

The conservation of mass in one dimension is given by the continuity equation:

$$\frac{\partial \rho}{\partial t} + \frac{\partial}{\partial x}(\rho u) = 0 \tag{10}$$

Where u is the flow velocity of a fluid.

Again linearizing the continuity equation yields:

$$\frac{\partial}{\partial t}(\rho_0 + \rho_0 s) + \frac{\partial}{\partial x}(\rho_0 u + \rho_0 s u) = 0 \tag{11}$$

Noting that density doesn't change with time or location and some further simplification produces the new continuity equation:

$$\frac{\partial s}{\partial t} + \frac{\partial u}{\partial x} = 0 \tag{12}$$

Lastly we consider Euler's force equation using material derivatives:

$$\rho \frac{du}{dt} + \frac{dP}{dx} = 0 \tag{13}$$

Linearizing the above equation yields:

$$(\rho_0 + \rho_0 s)(\frac{\partial}{\partial t} + u\frac{\partial}{\partial x})u + \frac{\partial}{\partial x}(P_0 + P) = 0 \tag{14}$$

Simplifying we obtain the one dimensional Euler force equation:

$$\rho_0 \frac{du}{dt} + \frac{dP}{dx} = 0 \tag{15}$$

The time derivative is then applied to the continuity equation as well as multiplying by ρ_0 and t the spatial derivative is applied to the force equation. The two equations are subtracted and the equation of state is substituted to produce:

$$\frac{-\rho_0}{B}\frac{\partial^2 p}{\partial t^2} + \frac{\partial^2 p}{\partial x^2} = 0 \tag{16}$$

Finally the acoustic wave equation for pressure is derived as:

$$\frac{\partial^2 p}{\partial x^2} + \frac{1}{c^2}\frac{\partial^2 p}{\partial t^2} = 0 \tag{17}$$

Where c is the speed of sound expressed in terms of the bulk modulus and density [39]:

$$c = \sqrt{\frac{B}{\rho_0}} \tag{18}$$

There are a multitude of methods to solve for the wave equation one of which involves the use of the method of separation of variables. Plane wave solutions using separation of variables in Cartesian coordinates (x, y, z) considering the boundary condition of the wave being fixed at both ends have the form:

$$p(x) = \sum_{n=1}^{\infty} \sin(\frac{n\pi x}{l}) \left[a_n \cos\left(\frac{n\pi ct}{l}\right) + b_n \sin\left(\frac{n\pi ct}{l}\right) \right] \quad (19)$$

Where a_n and b_n are amplitudes determined by the initial conditions of the wave, n is the index number starting after zero, l is the location of one end of the wave and x is the current location under consideration. The solution describes both a forward and backward travelling wave.

1.3.4 Time-of-Flight and Sound Speed [39]

When an ultrasonic wave pulse is directed perpendicular to several media interfaces, different signals are received based on the reflections from each of these interfaces. The time lapse between the signal's emission from and reception at the transducer is deemed the time-of-flight (TOF). TOF depends on many factors, including sound speed, thickness, density and temperature of the media. Based on the TOF between two separate interfaces, the sound speed (v) of that media can be determined by the simple equation:

$$v = \frac{2(thickness)}{TOF} \quad (20)$$

The factor of two in the numerator is included because the waves traverse twice the distance; once from the boundary, and once back. Some examples of sound speed in biological matter are outlined in Fig. 1.6. Human tissues tends to have relatively high water content, reducing their sound speeds while other materials such as metals tend to have stronger molecular bonds allowing increased speeds of wave propagation.

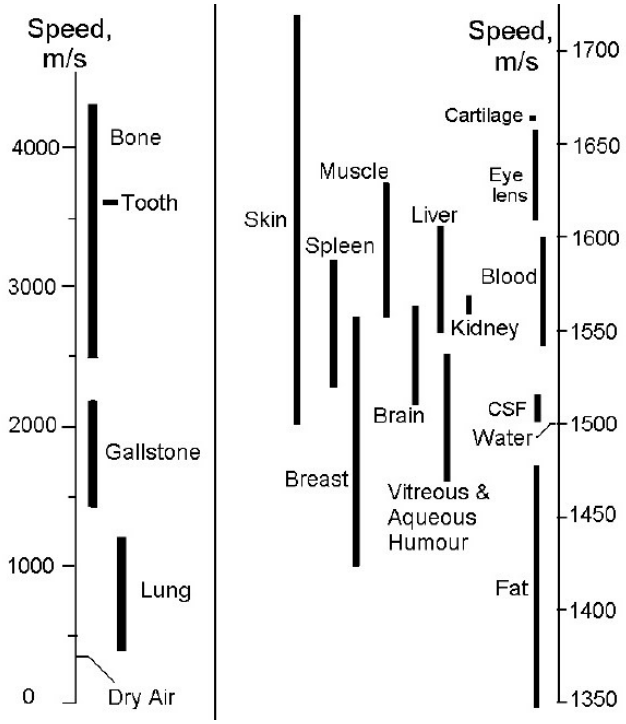

Figure 1.6: Sound speed of various tissue media subject to temperatures between 20-37°C [39].

1.3.5 Reflection, Transmission and Acoustic Impedance of Sound Waves [39]

Acoustical impedance (Z) is a common property of a media described by its density and sound speed:

$$Z = \rho v \tag{21}$$

This is a property that is dependent on both frequency and position, and influences wave propagation between media interfaces. When a wave makes contact with a medium of different acoustic impedance, its direction is altered due to the change in properties. Below in Table 1.3 are examples of the acoustic impedance of some common tissues:

Table 1.3: Acoustic impedance of common biological tissues and molecules.

Medium	Acoustic Impedance (MRayl)	Reference
Dry air (1 atm)	0.0004	[40]
Human fat	1.38	
Water (50°C)	1.54	
Human blood	1.61	
Human kidney	1.62	
Human muscle	1.70	
Cancellous human bone	1.54 - 2.2	[41]
Cortical human bone	4 - 8	

Reflectance (R) is defined as the ratio between the amplitudes of a reflected signal and that of its incident signal; similarly, transmittance (T) is defined as the ratio between the amplitudes of a transmitted signal and that of its incident signal. Together, reflectance and transmittance sum to 1 or 100% [39]:

$$R = \frac{A_r}{A_i} = \frac{Z_2 cos\theta_i - Z_1 cos\theta_t}{Z_2 cos\theta_i + Z_1 cos\theta_t} \tag{22}$$

$$T = \frac{A_t}{A_i} = \frac{2Z_2 cos\theta_i}{Z_2 cos\theta_i + Z_1 cos\theta_t} \tag{23}$$

Where Z_1 and Z_2 are the acoustic impedances of the first and second medium and θ_i and θ_t are the incident angle and transmitted angle of the wave.

The intensity of a propagating wave is given by [39]:

$$I = \frac{1}{T}\int_0^T P(t)v(t)dt \tag{24}$$

Where T is the period of the wave, P(t) is the pressure at a specific time and v(t) is the sound speed at a specific time.

This equation is reserved for a wave passing through an area perpendicular to the propagation direction. The intensity for a plane wave is modelled by [39]:

$$v(t) = \frac{P(t)}{c_0 \rho_0} \tag{25}$$

$$I = \frac{|P(t)|^2}{2 c_0 \rho_0} \tag{26}$$

Where c_0 is the reference sound speed, ρ_0 is the reference acoustic impedance and intensity is in units of average energy per unit area.

As mentioned previously, a wave may reflect and/or transmit at the arrival of an interface of media equipped with much different acoustic impedance than the previous media. This interaction can be modelled by Snell's law (Fig. 1.7) [39]:

$$\frac{sin\theta_i}{c_1} = \frac{sin\theta_r}{c_1} = \frac{sin\theta_t}{c_2} \tag{27}$$

Where $\theta_i, \theta_r, \theta_t$ are the angles of the incident, reflected and transmitted waves respectively, and c_1, c_2 are the wave velocities in medium 1 and 2. If the acoustic impedances of the two media are very different the reflectance will be large and transmittance small.

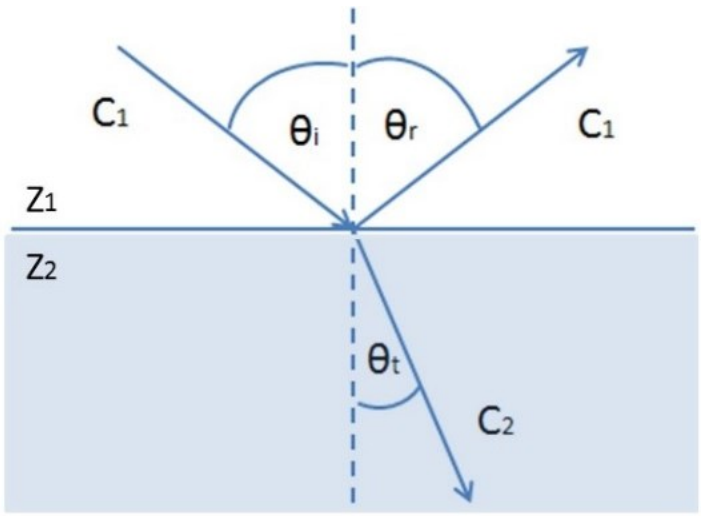

Figure 1.7: Ray diagram illustrating how an incoming ray is both reflected (r) and transmitted (t) when incident on a second media of different acoustic impedance.

1.3.6 Scattering, Absorption, Diffraction and Attenuation [39, 42]

In reality, most media are not 100% homogenous, and so it would be rare to describe a medium in which waves truly travel in entirely predictable directions. The incident waves will more realistically diverge from their straight path once in contact with the new medium, due to inevitable non-uniformities in compressibility, density or deformities along that trajectory in localized areas. The process is deemed scattering, and occurs in all forms of radiation including light and sound alike. The non-uniformities cause oblique reflections of the waves which will alter the data received from that object. To compensate for these reflections one must consider the field difference from before the object was present to when the object was introduced. For example, the total pressure field at a position x and time t should be:

$$p(x,t) = p_i(x,t) + p_s(x,t) \tag{28}$$

Where p_i is the incident pressure field with no object present and p_s is the scattered pressure field from the object.

Another form of information loss is from absorption, whereby a wave's energy is absorbed at the interface as opposed to being reflected. The absorbed energy is converted to heat, chemical energy or light, but also delivered throughout the object. In the case of this thesis, scattering and absorption were not taken into consideration for the sake of simplicity; however it is to be acknowledged that these phenomena contribute to signal error. The cumulative effects of absorption and scattering are considered in the process of attenuation. Attenuation takes into account the intensity loss after a beam of waves is transmitted through a medium, and is represented by the attenuation coefficient. The output intensity considering attenuation is given by:

$$I(x) = I(0)e^{-2\alpha x} \tag{29}$$

Where I(x) is the final intensity transmitted through the medium, I(0) is the initial intensity of the beam, α is the attenuation coefficient and x is the displacement through the medium.

The attenuation coefficient can be determined from the initial and transmitted intensities of pressure in units of N/cm-MHz or dB/cm-MHz. This can be performed if the attenuation coefficient is not extensively large so that p_0^2 is proportional to I_0:

$$\alpha_N = \frac{1}{2x} \ln \frac{I(0)}{I(x)} \tag{30}$$

Where α_N is given in units of N/cm-MHz in the above equation but can be converted to α_{dB} [db/cm-MHz] by multiplication of a factor $20\log_{10}(e)$.

Attenuation coefficients are dependent of frequency, temperature and pressure but are seen to be approximately linearly proportional to frequencies from 1-50 MHz and in soft tissues can be predicted roughly by 0.3 dB/cm-MHz [43].

Diffraction occurs when multiple interfaces are in the path of the sound wave. Due to the differing acoustic impedances and indices from refraction from the interfaces, sound waves 'bend' or alter their angle of traversal after entering a new medium. This causes slight deviations in the perceived measurements of a signal upon reception from several layers. For example, an incident beam normal to an interface will be seen to have the same TOF or thickness as the actual sample, since the angle of incidence is zero. Should that angle veer from zero, the perceived and actual thicknesses, or TOF's, will differ due to diffraction (Fig. 1.8). For small incident angles, as in the case of this thesis, the effects of diffraction can be disregarded.

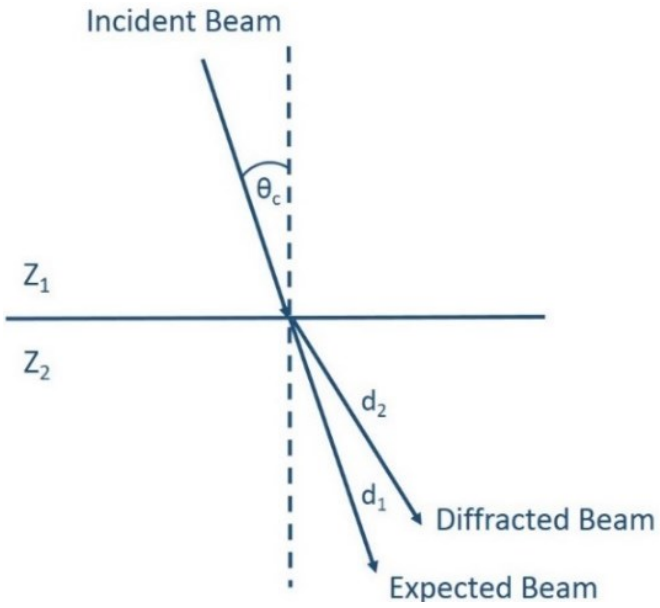

Figure 1.8: Diagram showing the effects of diffraction on one interface with different acoustic impedance. The ray d_1 is the expected propagation direction of the incident wave and the ray d_2 is the actual propagation direction due to diffraction.

1.3.7 Elasticity [42]

When a solid object is deformed by twisting, stretching or compression, its ability to restore back to its original shape is called elasticity. Applying stress to a solid such as a tension or compression equates to a force being applied per unit area. The amount of deformation due to a stress being applied is called strain, and is defined as the change in shape from its original configuration to an altered one. Stress and strain are proportional to each other by means of the modulus of elasticity, otherwise known as Young's modulus (E or Y).

$$E = \frac{stress}{strain} = \frac{FL}{A\Delta L} \tag{31}$$

Where F is the force, L is the original length of the solid, A is the area that is deformed and, ΔL is the change in length after deformation.

The speed of sound in an isotropic solid is related to the Young's modulus by:

$$v = \sqrt{\frac{E}{\rho}\frac{1-\sigma}{(1-2\sigma)(1+\sigma)}} \tag{32}$$

Where σ is Poisson's ratio.

If the cross-sectional area under deformation is very small in comparison to the wavelength of sound, then Poisson's ratio can be neglected and the equation simplifies to:

$$v = \sqrt{\frac{E}{\rho}} \tag{33}$$

1.3.8 Wave Types: Longitudinal, Transverse and Surface

As mentioned previously, the most basic wave formations are comprised of longitudinal and transverse waves that travel in the bulk of a medium. At the boundary of a solid-liquid or liquid-solid interface there are several types of acoustic waves that are produced. Longitudinal waves are present within angles less than the critical angle. At angles completely or almost perpendicular to a different boundary, longitudinal waves dominate and yield the strongest energy intensity as shown in Fig. 1.9. Transverse or shear waves are created due to the stress and strain induced by the incident wave on a solid isotropic medium. These waves are produced at angles equal to and larger than the critical angle from a liquid to solid (smaller to larger impedance changes). The incident wave causes vibrations and distortions in the molecular structure of the solid creating lateral displacement among particles perpendicular to the propagation direction and forming a shear wave.

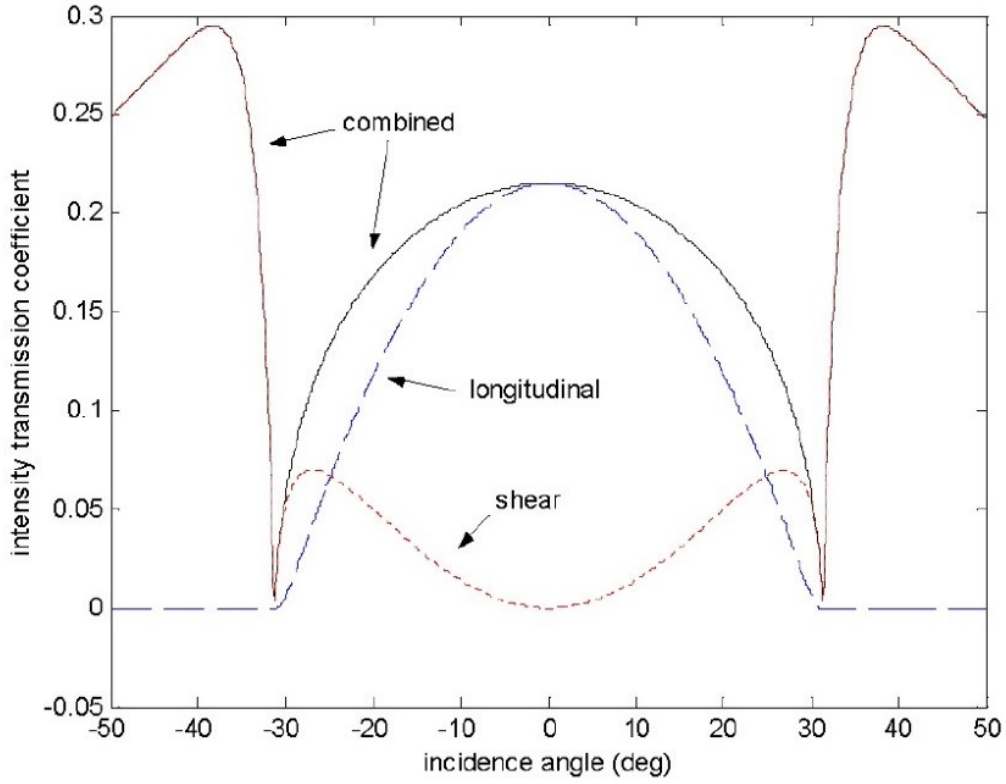

Figure 1.9: Graph showing the intensity of longitudinal and shear waves based on incident angle [44].

Unlike longitudinal waves, shear waves can be polarized in any direction; thus, shear waves yield greater sensitivity toward detecting even the smallest structural deformities. The longitudinal sound speed and shear sound speed are related by [39]:

$$\frac{C_L}{C_S} = \sqrt{\frac{2(1-\sigma)}{1-2\sigma}} \tag{34}$$

Where C_L is the longitudinal sound speed, C_S is the shear sound speed and σ is Poisson's ratio.

The remaining wave type in solids is the surface wave, or Rayleigh wave, named after Lord Rayleigh in 1885 [39]. This is a wave that propagates along the surface of the solid interface and does not penetrate far - only up to one wavelength in depth [39]. These waves include both longitudinal and transverse motion meaning the particle motion is along an elliptical outward motion and decreases exponentially with distance [45]. These waves are mainly used to inspect surface defects of solid materials with high

sensitivity. Rayleigh wave sound speed is slightly smaller than shear wave sound speed and can be approximated through an equation by Viktorov [45]:

$$K = \frac{C_R}{C_S} = \frac{0.87 + 1.12\sigma}{1 + \sigma} \tag{35}$$

Where C_R is the Rayleigh sound speed.

1.3.9 Near and Far Field Effects

When considering the behaviors of a focused ultrasonic beam one must distinguish between the near field (Fresnel region) and far field (Fraunhofer region) based on the location of the point of observation. Different effects are apparent in these regions due to dispersion of the beam over distance. The far-field region is defined as Equation (36) and the near-field region is defined as Equation (37). In the far-field, the beam intensity contains more uniformity due to larger divergence of the beam while in the near-field, beam intensity is more varied due to more focusing.

$$a >> r^2 f \qquad far - field \tag{36}$$

$$a << r^2 f \qquad near - field \tag{37}$$

Where a is the location of viewing, r is the transducer radius and f is the frequency.

Between these two regions there is an area of focus deemed the focal zone. This intermediate region provides the narrowest beam width and greatest beam focus. It takes part half in the far-field and half in the near-field. Within the focal zone there is a spot of maximum focus called the focal point. This is the optimal location for imaging in ultrasound because it provides the greatest intensity and resolution.

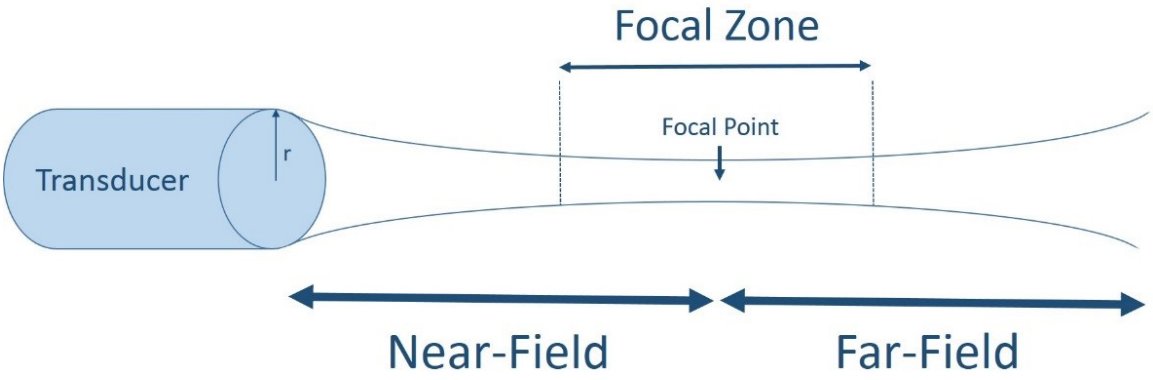

Figure 1.10: Diagram of the regions within a focused ultrasonic beam from a transducer with radius 'r'. These regions are outlined as the near-field, far-field and focal zone where the focal point is the single point of maximum lateral resolution along the beam.

Chapter 2 PRELUSIVE FINGERNAIL ASSESSEMENT – A CLINICAL DATA COLLECTION

Summary: This chapter aims to investigate whether fingernail defects are identifiable by conducting a preliminary data collection survey on patients receiving chemotherapy. It also outlines the first of the two methods of investigation used in this thesis to characterize properties of fingernails with ultrasound.

2.1 Investigation of Chemotherapy Affected Fingernails

As mentioned previously, fingernails may provide valuable information about the health of the human body, and so, the exploration of their changes due to harmful effects on the body was of interest. A preliminary survey was conducted on patients receiving chemotherapy to examine whether chemotherapeutic treatments are correlated with the physical effects observed on the fingernails as described in literature. This was to be done by demographic, neuropathy and ultrasonic assessments. This application could provide more insight into the limited investigation of using ultrasound to study chemotherapeutic effects [13]. The investigation of the changes occurring on the fingernails via ultrasonic measurement is a possible quantitative method for assessing the development and severity of one's bodily response to chemotherapeutic treatment adjunctive to current clinical examination methods. The benefits of high frequency ultrasound include the fact that it is non-invasive, provides increased resolution of nail plate echogenicity, and does not induce harmful radiation. This article provides initial evidence that ultrasound can be used to assess the relationship between the harmfulness of anticancer drugs to the body, and the changes in fingernail TOF magnitude over successive measurements during treatment. Ultrasound has been shown to be an effective method of assessing ungual properties in cases of normal, healthy patients and those affected by skin diseases, as validated by several sources; however, this is the first instance in which ultrasound has

been applied in the exclusive investigation of the effects of chemotherapy on the fingernail. [18, 29, 30, 31, 46].

2.2 Fingernail Deformities Caused by Chemotherapeutic Treatment

Fingernails are affected by many factors, from alterations within the body to external influences such as the environment. One case of interest is the effects on fingernails during chemotherapeutic treatment. Chemotherapy involves the intravenous administration of anticancer agents in effort to eradicate proliferating cancer cells. The distribution of these drugs induces many adverse reactions throughout the body such as those seen in fingernails, which include: onycholysis, discoloration, Muehrcke's lines, splinter hemorrhage, subungual hematoma and complete nail fracturing or detachment [47, 48, 49, 50]. Figure 2.1 illustrates some of the likely defects observed during cancer treatment and Table 2.1 describes various defects likely present during chemotherapy.

Chemotherapy is the treatment of cancer by means of administering cytotoxic drugs to eradicate tumors [46, 51, 52, 53]. Taxanes are a group of antitumor drugs that include Paclitaxel and Docetaxel; these drugs effectively prevent cell division by altering the formation and disassembly of microtubules [54]. The treatment of cancer with chemotherapeutic drugs is often coupled with a series of adverse effects due to the damage caused to surrounding healthy cells. As previously stated, the effects of chemotherapy on the body extend to the nails via the vascular system, whereby blood flow complications such as hemorrhages or subungual hematomas may ensue [47, 55, 56]. It has been proposed that the harmfulness of certain drugs to the body can be determined by the extent of damage and changes detected in the nails [28]. During the advancement of these defects over time, the patient will likely experience discomfort and pain from inflammation of subungual or external tissue, nail thinning or cracking, nail detachment exposing the soft nail bed, numbness at the fingertips, and a loss in grip [47].

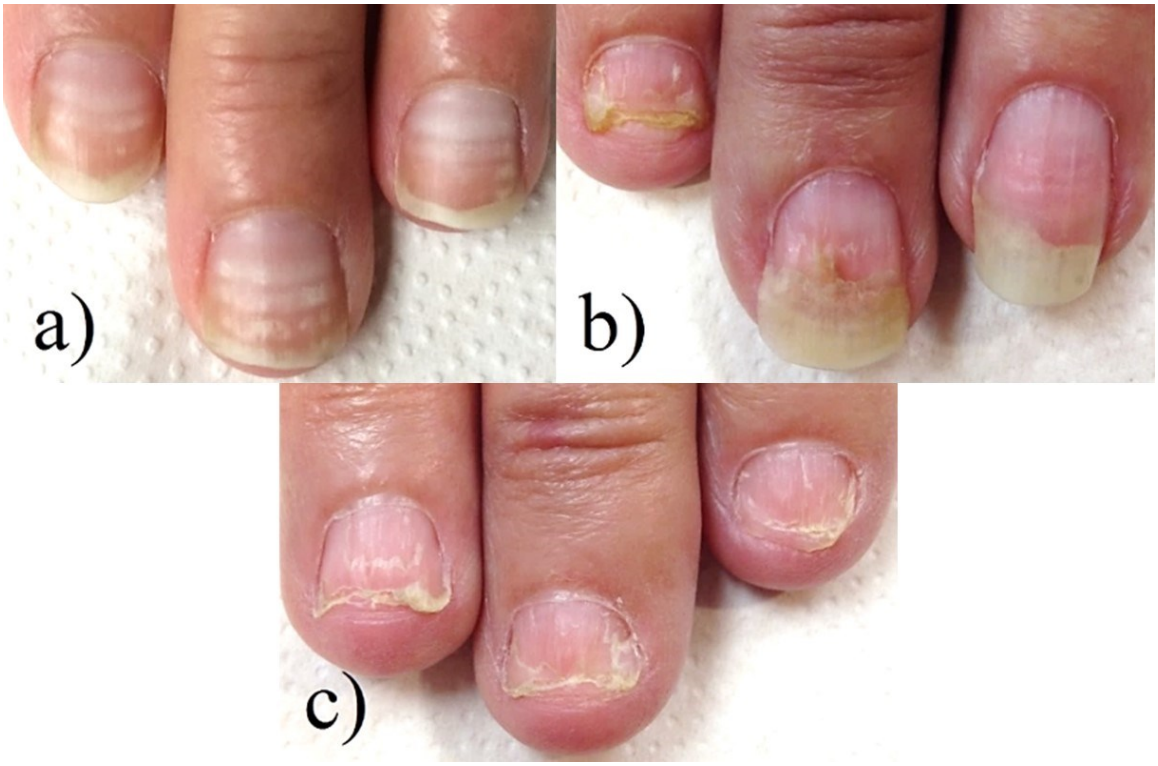

Figure 2.1: Examples of fingernail deformities showing a) Mee's lines b) onycholysis and c) nail fracturing/ detachment from three different patients from the data collection.

Table 2.1: General defects that arise in the fingernails according to literature [47].

Nail Defect	Definition
Mee's Lines	White transverse lines across nail plate
Beau's Lines	Traverse groves or ridges across nail plate
Muehrcke's Lines	White traverse lines across nail plate separated by pink nail bed
Onycholysis	Nail plate separation from nail bed
Subungual Hematoma	Hemorrhage of the nail bed (red or black color)
Onychomadesis	Longitudinal groove in the center of the nail plate
Splinter Hemorrhage	Many small, longitudinal brown lines at distal end of nail bed
Paronychia	Inflammation and discoloration of proximal nail fold

2.3 Materials and Methods of Clinical Fingernail Investigation

2.3.1 Subject Selection Criteria

The number of patients participating in this data collection was limited to those consenting to the research and undergoing taxane regimens. The patients were allowed to have previously received Adriamycin and Cyclophosphamide (AC) but no other form of chemotherapy. This data collection was focused on patients with taxane (Docetaxel/Taxol and Paclitaxel/Taxotere) as part of their weekly or biweekly regimens ranging from 6 to12 week regimen periods. This study was approved by the ethics committee of the Metropolitan Hospital in Windsor, Ontario, and the University of Windsor. The measurements were performed *in-vivo* on patients of any age demographic and any ethnicity. Other medical conditions were not considered in the criteria and previously damaged nails were included.

2.3.2 Study Procedure

The ultrasonic system used in this study operated in real-time, pulse-echo mode with a transducer central frequency of 50 MHz and 7 mm focal length. Using water as the coupling medium between the transducer tip and patient's fingernail, B-scans were taken on two fingers from each hand: left and right index fingers, and left and right middle fingers. These fingers were chosen due to their fastest growth rates which would likely show earliest signs of defects [17]. The nail surface was held steady by inserting the finger into a holder designed to limit its movement. The transducer was aligned to the middle of the selected nail closest to the cuticle at the beginning of each measurement. Once satisfactory signals of maximum amplitude were obtained from reflections at both the surface of the nail plate and the interface between the nail plate and nail bed, a B-scan was initiated across the fingernail, starting partially on the cuticle closest to the proximal nail fold and ending slightly past the edge of the fingernail. During this time, the patient remained completely motionless so as to avoid disrupting the scan. The total distance traversed by the transducer across the fingernail was 16 mm. Photographs were also taken after each measurement to monitor visible changes in the ungual structure and

discoloration of the nail bed or nail matrix. Three sets of measurements were taken for each patient: starting before taxane treatment, in the middle of treatment and on the last day of treatment.

Upon completion of the three sets of measurements, B-scans were compiled and a two-dimensional grayscale image was generated. Starting closest to the cuticle, A-scans were selected to measure the TOF from the top surface of the nail plate to the interface between the nail plate and nail bed as shown in Fig. 2.2. Nail density, hydration and thickness may change in the presence of diseases, causing alterations in the speed with which the ultrasonic waves propagate through the nail; thus, since the speed of sound is not uniform throughout the nail, this study reports measurements in terms of TOF rather than thickness. [17, 28].

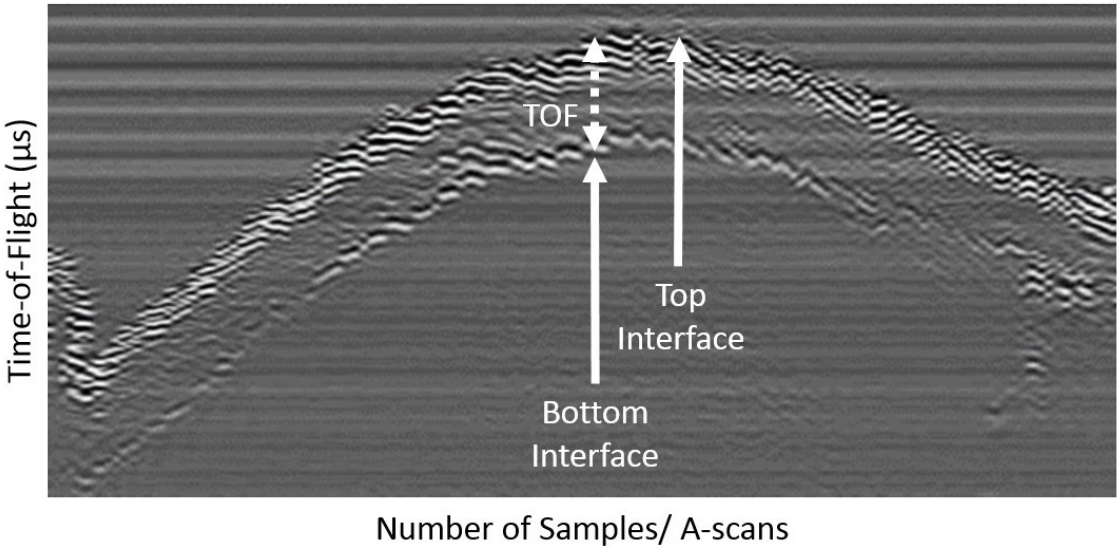

Figure 2.2: B-scan of fingernail outlining the TOF between the top and bottom interfaces. The vertical axis represents the TOF amplitude in gray-scale values and the horizontal axis represents the number of A-scans traversed along a fingernail from cuticle to distal end. The two darker curves represent the top and bottom fingernail boundaries.

2.4 Device Prototype Design

To accommodate an ultrasonic transducer to our application on fingernails, a finger holder was required to sit comfortably and reliably on top of the fingernail. A custom carcass was designed and 3D printed to personal specifications of size and shape to allow

greatest usability and transducer motion. The holder allowed the transducer to translate forward and backward, as well as up and down to attain focus at the focal point. A spring-loaded actuator stepper motor was attached to allow complete control of displacement speed and distance by user specifications via software coding. The stepper motor was regulated by a controller board which was also connected to a laptop or tablet display.

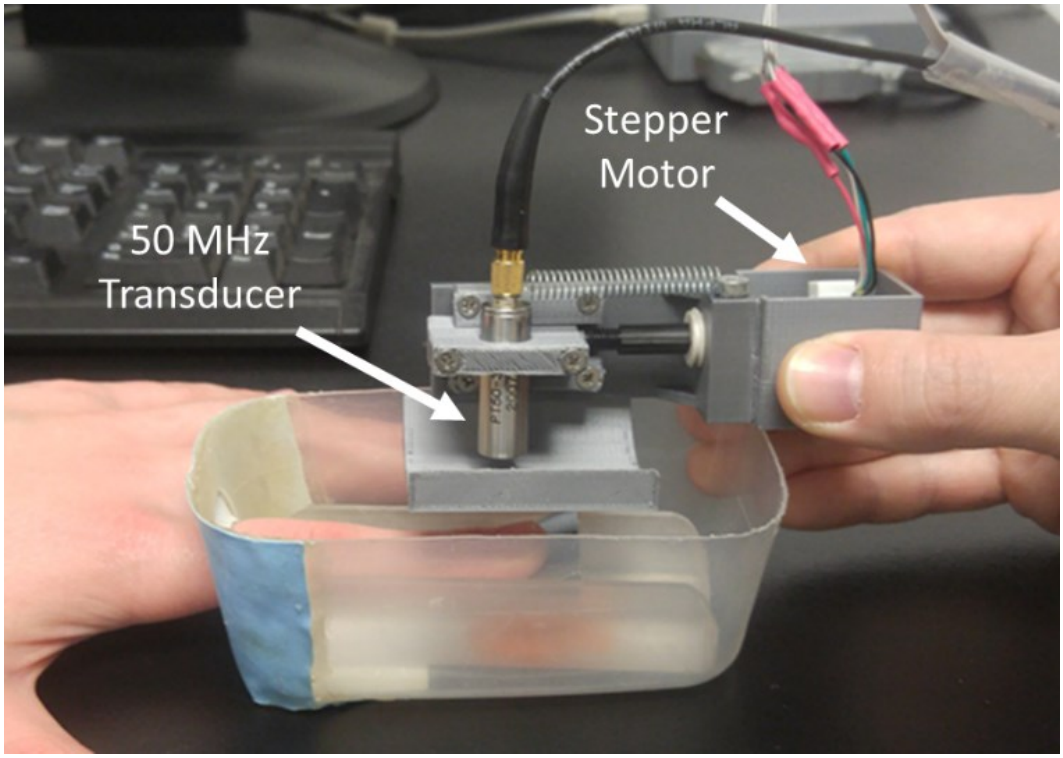

Figure 2.3: Ultrasound prototype for fingernail assessment in data collection. The 50 MHz transducer was attached to a 3D printed carcass and a spring-loaded stepper motor to allow B-scans to be taken longitudinally across the fingernail. A container was also made so that the fingernail can be inserted and submersed in water to act as the impedance matching layer to the transducer.

2.5 Transducer Parameters and Setup for Resolution Calculation

A 50 MHz transducer was custom-ordered to meet our requirements based on transducer frequency and cost. The frequency was chosen due to several reasons. In order to view fingernail microstructure, we required a wavelength of at least 200 µm but with as high resolution as possible provided by a high ultrasonic frequency. Also, given high attenuation in keratin, the reflected ultrasound intensity must be high enough at a

maximum fingernail thickness depth of minimum 1 mm. Longitudinal waves were of interest for this data collection as opposed to transverse waves for two reasons: first, because of the high attenuation of keratin in fingernails, and second, since such high frequency waves would cause a faster signal decay along larger distances that would be required in shear methods. Also, the roundness of the fingernail would cause unnecessary difficulty in patient positioning for detecting shear waves. Ultimately, for the parameters of interest, longitudinal waves what would be required with transverse waves. Also the roundness of the fingernail would cause extra problems in positioning for detection of shear waves. Further testing was done on the transducer to determine the lateral and axial resolution of the ultrasonic beam produced. This was accomplished with the use of a motorized displacement arm attached to a hydrophone, or pinducer, in a large water bath (Fig. 2.4). The pinducer was model Onda HGL-0400 with 0.25-20 MHz broadband frequency range at ±3 dB of the signal amplitude and 400 μm aperture size. The sampling frequency for the pinducer was 2.5×10^9 Hz. A pulse generator and trigger generator were attached to both transducers to ensure signal timing was coordinated to allow sending and receiving from each end. The pulse generator operated at 100V with a pulse repetition rate of 200 Hz. Due to the nature of the pinducer, low-pass and high-pass filters were applied to limit its frequency range to 1-20 MHz. According to the pinducer data sheet provided with its purchase the amplitude error associated with using frequencies 0.5-1 MHz are ±1.5 dB, 1-15 MHz are ±1 dB and 15-20 MHz are ±2.2 dB.

The motorized arm allowed precise movement of the pinducer in three dimensions. The transducer was first carefully aligned to directly face the tip of the pinducer. The robotic arm then moved in a plane axial to the transducer beam up, down and backward, starting closest to the transducer surface and moving away. The pressure distribution of the ultrasonic beam in water was recorded and the focal area and focal spot were determined from MatLab software. The axial and lateral displacements of the robotic arm were set to the smallest possible values on the software, which corresponded to 0.25 mm in both directions. The beam distribution was then plotted based on the normalized pressure within a color image (Fig. 2.5). The image shows the focal zone as well as the focal spot. The red region shows the highest intensity, and the white dot represents the pixel with maximum intensity corresponding to the focal spot in water. The

white dashed line is along the lateral direction of the beam and helps pinpoint the location of the focal spot. By using the sound speed of 1482 m/s and density 1000 kg/m^3 of water, the focal distance was calculated to be 7.0±0.1 mm. For collision safety precautions, the pinducer was not able to be touching or too close to the transducer tip; hence, the x-axis of Fig. 2.5 does not start at zero. The lateral focal zone of the beam intensity was calculated along the white dashed line and at -6 dB of the normal Gaussian beam distribution corresponding to the full width half maximum (FWHM) (Fig. 2.6). This value of lateral focal zone FWHM was calculated to be 2.1±0.1 mm. The axial focal zone of the beam intensity was calculated perpendicular to the white dashed line and at -6 dB of the normal Gaussian beam distribution corresponding to the full width half maximum (FWHM) (Fig. 2.7). This value of axial focal zone FWHM was calculated to be 3.9±0.1 mm.

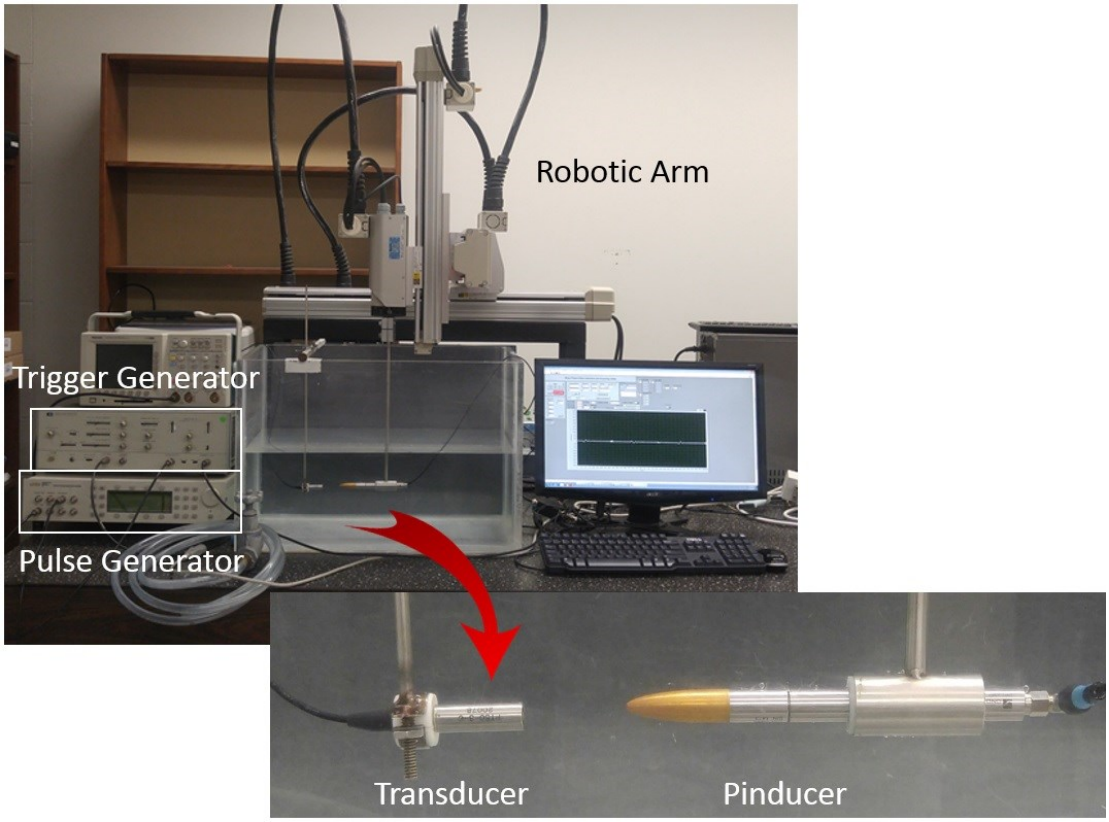

Figure 2.4: Diagram showing the setup used to determine transducer resolution using a robotic moving arm, pulse generator, trigger generator, pinducer, 50 MHz transducer and display monitor. The pinducer was placed as to directly face the transducer and align in all three dimensions.

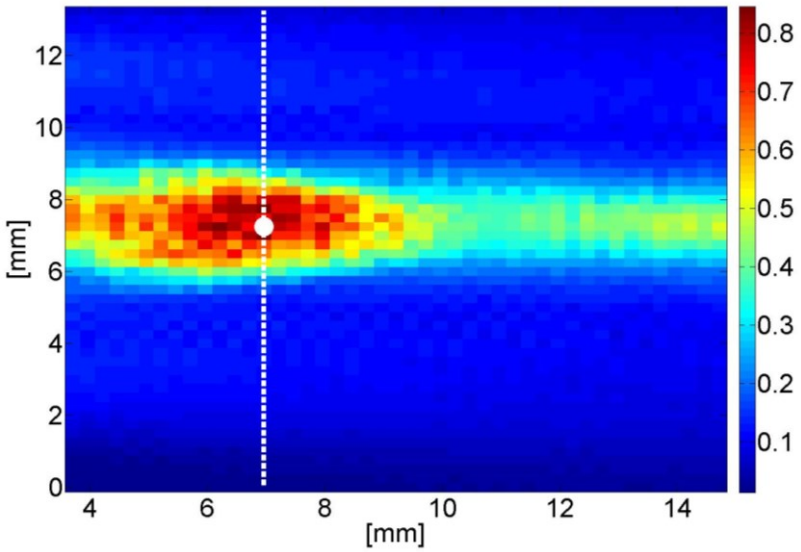

Figure 2.5: Normalized intensity distribution of transducer beam in water. The transducer emitting surface is to the left and the beam propagates to the right. The white dot represents the focal spot and the white dashed line represents the lateral distribution at the focal spot of the beam. Red represents the highest intensity and blue represents the lowest.

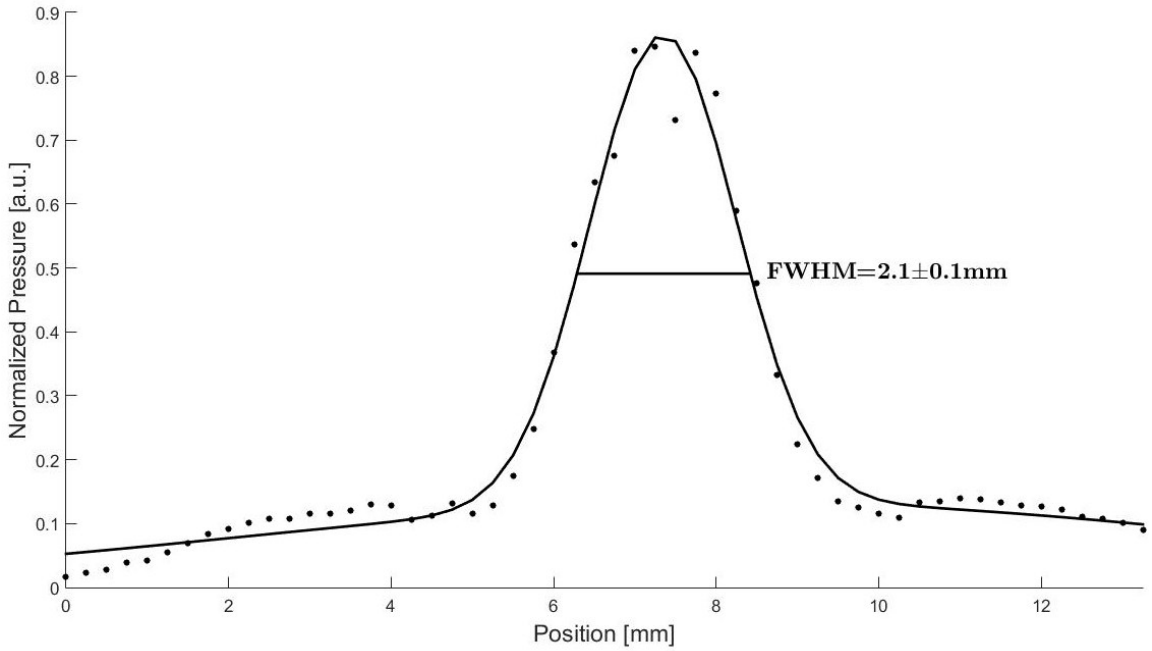

Figure 2.6: Beam distribution along the lateral focal zone at the focal spot for the FWHM. The black dots depict individual data points and the black solid line depicts the fitted Gaussian to the data points.

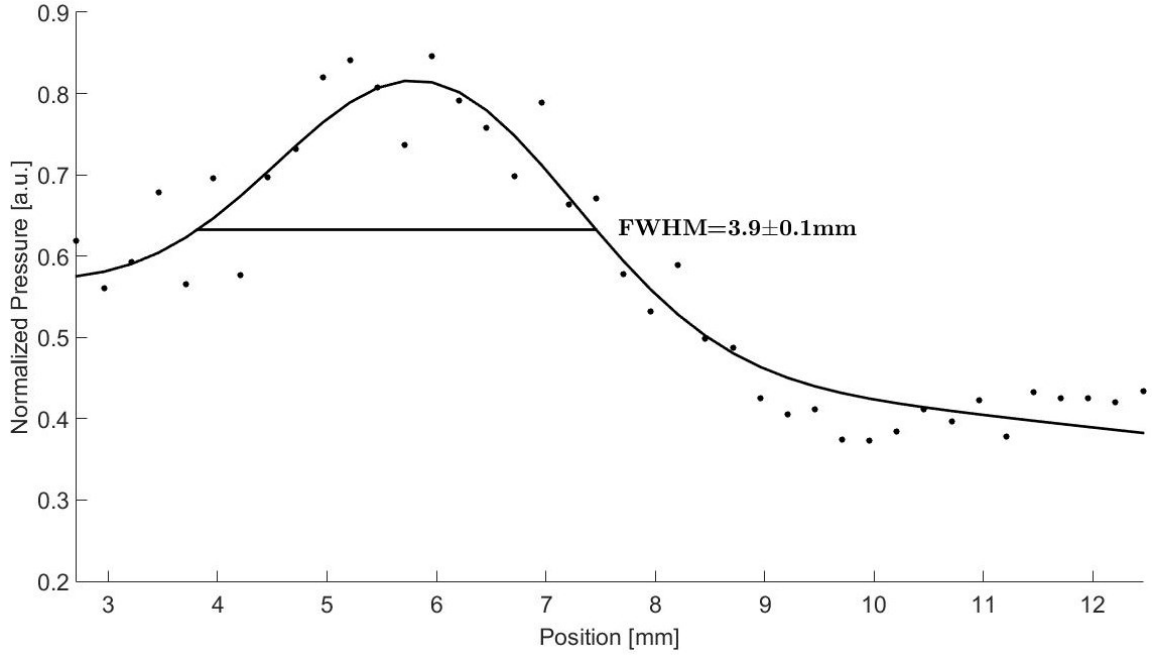

Figure 2.7: Beam distribution along the axial focal zone at the focal spot for the FWHM. The black dots depict individual data points and the black solid line depicts the fitted Gaussian to the data points.

The axial resolution of the transducer was calculated using a wave pulse emitted from the transducer. The wave was modelled as a Gaussian wave, and the axial resolution was determined as the FWHM at -6 dB of the Gaussian peak. As an example, the axial resolution of the 50 MHz transducer was calculated according to the pulse obtained from Fig. 2.8. The axial resolution at -6 dB of the Gaussian distribution of the wave pulse was determined to be 0.08±0.01 mm. The lateral resolution is the same as the lateral focal depth which in water was 2.1±0.1 mm.

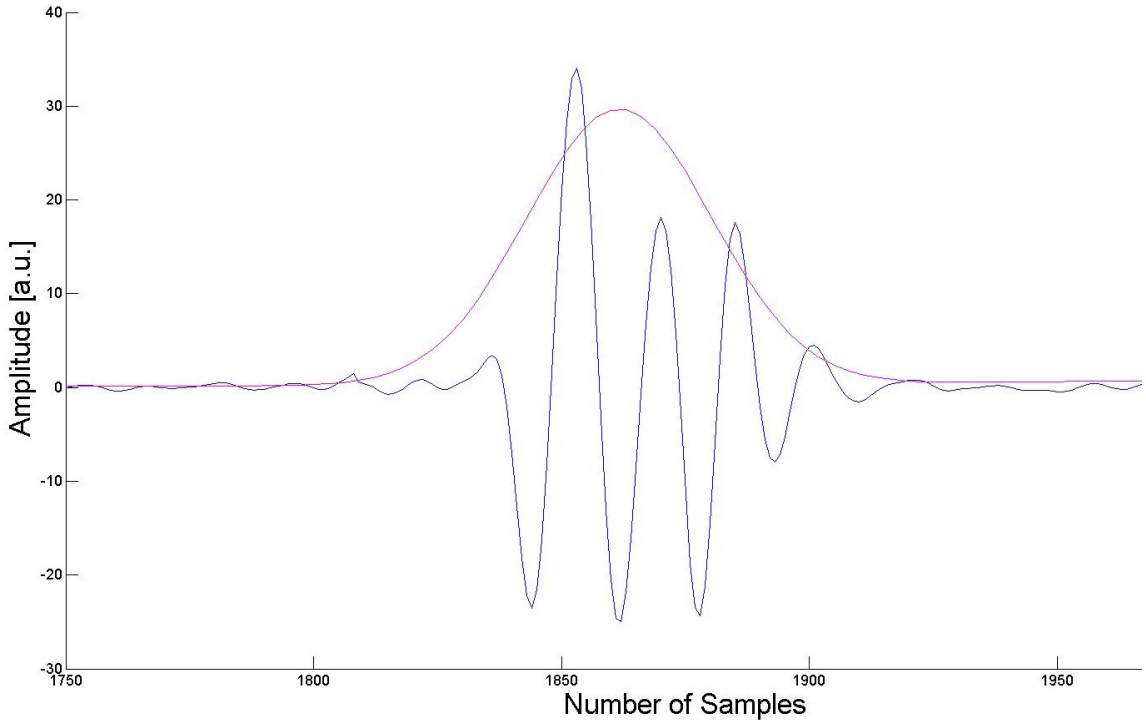

Figure 2.8: Graph showing a single pulse formation in blue from the 50 MHz transducer. The red line is the Gaussian distribution for this pulse in the axial direction.

Other parameters of the transducer, as well as values specified by the user, are provided in Table 2.2. This includes software parameters such as driving voltage, pulse length, number of samples, pulse repetition frequency, gain, delay time and sample averaging. Hardware parameters not mentioned previously include the type of piezoelectric material used for pulse excitation and the aperture size of the transducer front surface.

Table 2.2: Transducer parameters.

Parameter	Result
Central frequency	50 MHz
Number of elements	1 element
Focusing type	Spherical
Piezoelectric material	PVDF
Focal distance	7.0±0.1 mm
Aperture size	3 mm
Driving voltage	50 V
Pulse length	32 ns
Number of samples per a-scan	2048
Pulse repetition frequency	60 µs
Gain	+32 dB
Delay time	3.5 µs
Averaging	8 points
Lateral focal zone	2.1±0.1 mm
Axial focal zone	3.9±0.1 mm
Axial resolution	0.08±0.01 mm
Lateral resolution	2.1±0.1 mm

2.6 Results of Data Collection

2.6.1 Patient Demographics

In total there were 17 patients tested in the study, including 16 female and 1 male. The ages ranged from 35–69 years (mean 54.8 years), with ages 35-49 years accounting for 19% of volunteers, 50-59 years accounting for 50%, and over 60 years accounting for 31%. All of the patients were being treated for breast cancer with Paclitaxel in their regimen; none received Docetaxel. Demographics for each patient are shown in Table 2.3. Some patients underwent increases or decreases in dosage at the discretion of the oncologist; this is depicted in the Table by two values for taxane dosage. An increase in dosage meant the patient was experiencing minimal benefit from the chemotherapy and thus needed a stronger dose; conversely, severe adverse effects indicated lowering of

the dosage by the oncologist. In addition, the patients were divided into groups of weekly or biweekly dosed partitions.

Table 2.3: Patient demographics in order of youngest to oldest for each dosage frequency where F denotes female and M denotes male.

Dosage Frequency	Age (years)	Sex	Weight (kg)	Taxane Dose (mg)
Weekly	35	F	64	136
	38	F	87	147-118
	42	F	89	158-161
	50	F	61	130
	51	F	91	162
	65	F	68	145-87
	67	F	58	139-100
	68	F	46	108
Biweekly	51	F	74	309-324
	52	M	81	343
	53	F	67	309
	54	F	65	291
	55	F	49	255
	58	F	67	300
	60	F	95	350-315
	64	F	78	327
	69	F	79	342-330

2.6.2 Qualitative Observations

Literature review showed evidence that taxane and Paclitaxel administration caused pain and discomfort in the hands of chemotherapy patients. This lead to the incorporation of a qualitative grading scale in our measurements to assess such effects, in effort to confirm with literature observations. Both visual and verbal assessments were conducted on all patients. Also, photographs were taken during each measurement, and questions were asked about changes in grip strength and sensations of numbness at the fingertips. Fingertip numbness and grip strength questions were based on a NCI CTC v.3 (National Cancer Institute Common Toxicity Criteria Version 3) grading scale from 0-4, where zero represents no change and four represents a drastic change [57]. This is a popular neuropathy scale used in the medical field to assess the severity of pain sensitivity based on the opinion of the patient. The defects visually observed for all of the

patients by means of photographs are outlined in Table 2.4. The main fingernail abnormalities that occurred in patients of this study were onycholysis, fingernail discoloration, white transverse lines, white lunula, discolorations and fracturing or partial detachment of the fingernail. It was not evident whether transverse lines or discolorations were limited to the nail bed, or to the fingernail plate, or present simultaneously in each. It was also not evident whether the transverse lines remained in the same locations over time (meaning the abnormality existed in the nail bed), or if they shifted as the fingernails grew (meaning the abnormality could be linked to the fingernail plate). The study showed that 47% of patients developed onycholysis and/or discoloration and 24% developed white transverse lines and/or white lunula. There were some cases of patients whose fingernails broke off partially at different periods of treatment; those patients were excluded from the results since not enough data was available to conclude useful observations.

Table 2.4: Presence of total fingernail defects after treatment for weekly and biweekly dosed patients arranged in order from youngest to oldest (note that the — signifies that no fingernail defects were recorded)

Dosage Frequency	Age (years)	Onycholysis (detachment and/or discoloration)	White Transverse Lines and/or White Lunula
Weekly	35	●	
	38	●	
	42	●	
	50	—	—
	51		●
	65	●	
	67	—	—
	68	●	
Biweekly	51	—	—
	52	—	—
	53		●
	54	—	—
	55	●	●
	58	—	—
	60		●
	64	●	
	69	●	

The neuropathy assessment revealed that the majority of patients experienced a drastic change in sensation at their fingertips; chiefly, numbness. It was observed based on Figure 2.9-2.12 that numbness and grip strength worsened over each measurement, and for many cases became very severe. The worst cases of both grip strength and numbness were present in patients with ages 50+; this may indicate that chemotherapy adversely affects the nervous systems of this demographic more so than those of younger patients. This could serve as an early warning sign to reduce dosage quantities of Paclitaxel. Fingertip numbness was found to become quite intense, starting halfway into treatment and continuing until the end. Grip also worsened over the first half of treatment but did not worsen as quickly as the severity in numbness. Some patients did not begin with a scaling point of 0 because of previous injury, such as work accidents and previous adverse effects of AC treatment. By the end of treatment, many patients by the end of treatment complained of difficulties in manual dexterity, such as fastening buttons, opening pop tabs, twisting door knobs and lifting small or heavy objects with their fingers. All of the visual characteristics of onycholysis, nail discoloration and white transverse lines correspond with the literature observations for taxanes. Likewise, the change in grip strength and fingertip numbness were also comparable to those of previous studies on neuropathy of chemotherapy patients.

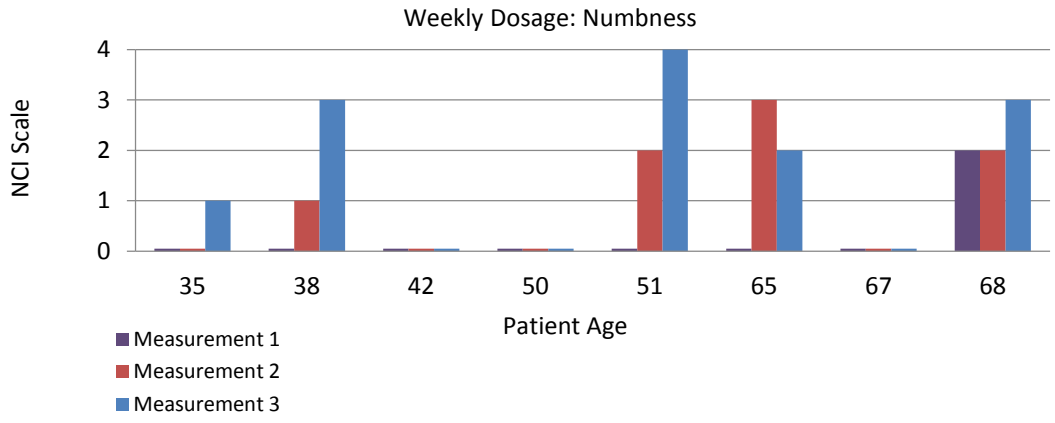

Figure 2.9: Weekly dosed numbness neuropathy: Bar graph of weekly dosed patients in order of age and their fingertip numbness response for each of the three measurements.

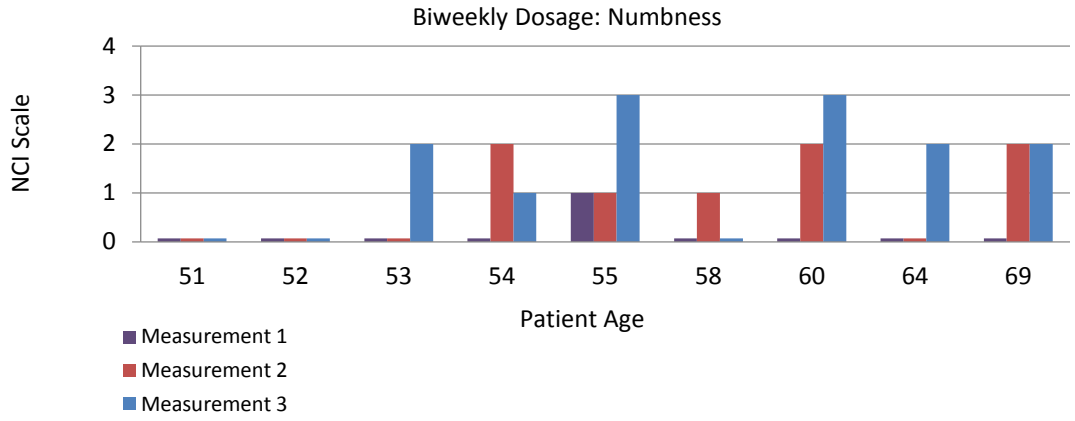

Figure 2.10: Biweekly dosed numbness neuropathy: Bar graph of biweekly dosed patients in order of age and corresponding fingertip numbness response for each of the three measurements.

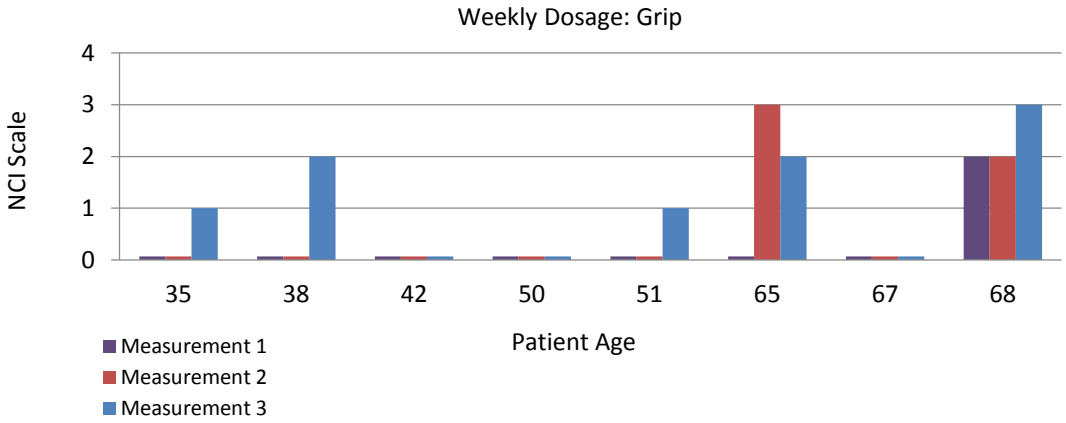

Figure 2.11: Weekly dosed grip neuropathy: Bar graph of weekly dosed patients in order of age and corresponding fingertip grip response for each of the three measurements.

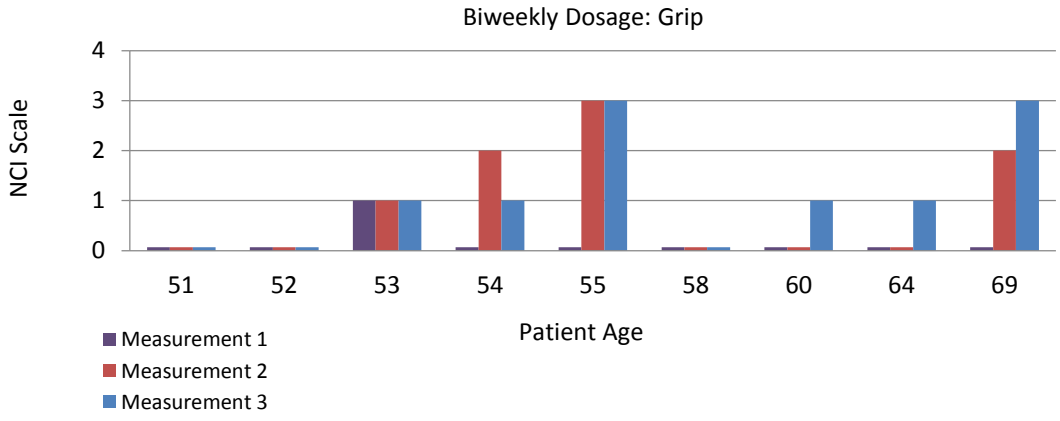

Figure 2.12: Biweekly dosed grip neuropathy: Bar graph of biweekly dosed patients in order of age and corresponding fingertip grip response for each of the three measurements.

2.6.3 Quantitative TOF Results

After acquiring data from three sets of measurements for each patient, the data was organized based on each hand's fingernails. Starting from the cuticle to 3.5 mm distally outward the first 10 A-scans were utilized to determine the TOF (in microseconds) of the fingernails. The 10 TOF values for each measurement period were plotted using box plots. In total, there are 4 box plots for each of the 17 patients. Examples of two of the patient's fingernail box plots are shown in Fig. 2.13 and Fig. 2.14. Patterns were determined for each of the three measurements periods based on TOF fluctuation changes for all patients. Patients with both weekly and biweekly treatment plans experienced a general decrease in the median TOF in each fingernail from the first half of their total regimen period. This was observed in 50% of the weekly dosed and 100% of the biweekly dosed patients. For the time period between the middle and end of treatment the median patient TOF in each fingernail was determined to be in general an increase. This was observed in 86% of the weekly dosed and 88% of the biweekly dosed patients. Finally, the baseline pre-treatment TOF median of the first 10 proximal A-scans in each fingernail were determined to have increased compared to those at the end of treatment. This was observed in 75% of the weekly dosed and 50% biweekly of the dosed patients.

Based on statistical analysis of the entire patient pool's fingernail measurements, it was determined that 68% of the measurement differences were deemed statistically significant according to two-sample t-tests. This was based on a 95% confidence interval which was deemed the limit for statistical significance. This analysis involved matching the TOF values obtained at the same fingernail locations with different measurement times to correlate their relevance.

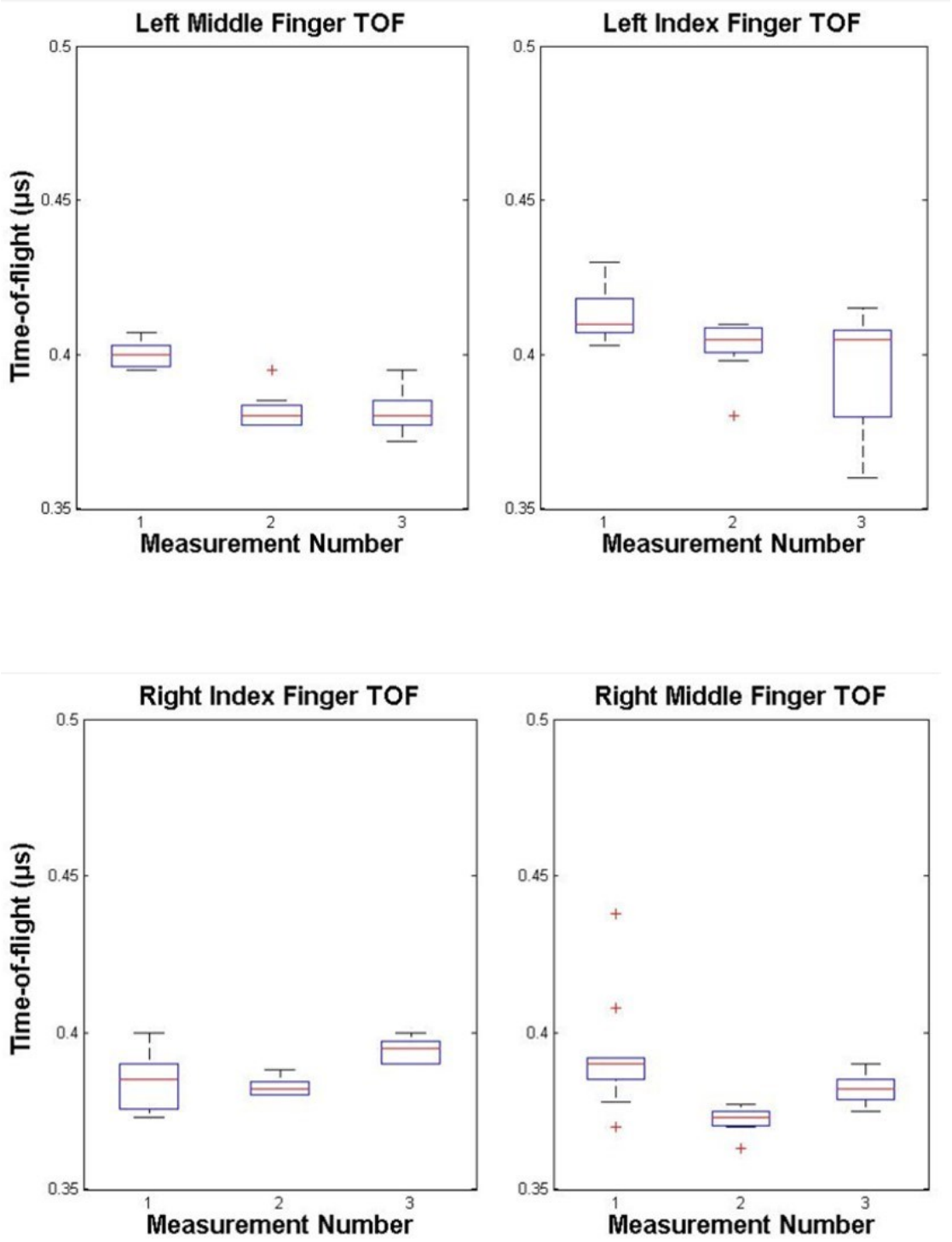

Figure 2.13: Patient A Fingernail TOF magnitudes: Boxplots showing TOF values for each measurement on the left middle, left index, right index and right middle finger of a 51 year old patient undergoing weekly dosing of taxane.

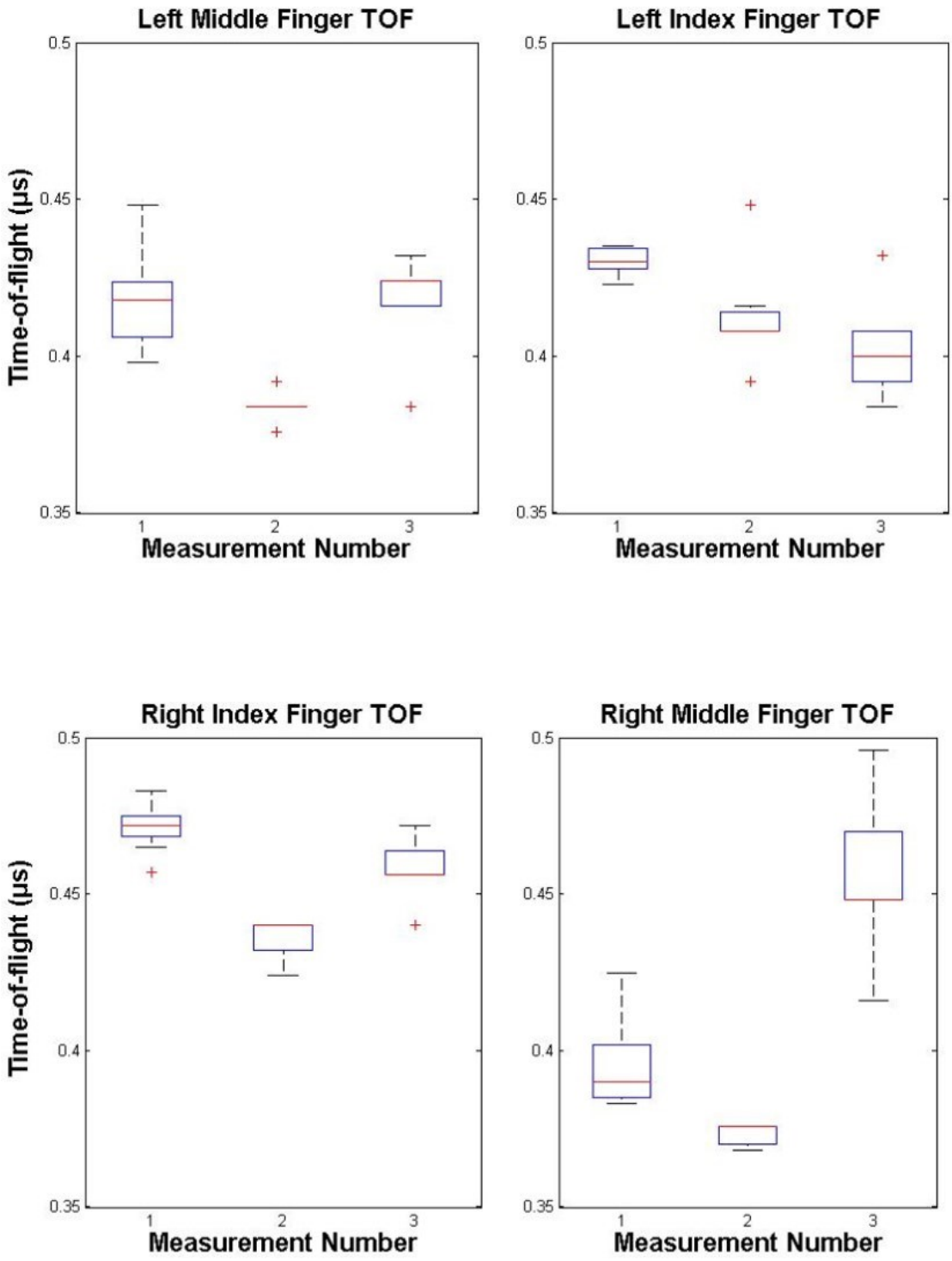

Figure 2.14: Patient B Fingernail TOF magnitudes: Boxplots showing TOF values for each measurement on the left middle, left index, right index and right middle finger of a 58 year old patient undergoing biweekly dosing of taxane.

2.7 Discussion and Conclusion of Study

This study suggests the use of ultrasound to assess the degree of chemotherapeutic toxicity to the fingernails, as an adjunct to current clinical methods of evaluating the patient's systemic health. Combining these techniques may result in higher patient satisfaction, reduced risks of fingernail discomfort and cosmetic flaws, as well as establishing earlier prognoses of chemotherapy regimen outcomes.

During the course of this study, it was observed that nail detachment or onycholysis became present in patients most prevalently at the distal and lateral portions of the fingernail. Thus, the proximal portion from where the fingernail grows appears not as affected as the already-grown fingernail at the distal portion. Although there were TOF differences seen throughout regimens, it was observed that the TOF values for the same patient were similar before treatment and by the last measurement. It was observed that discoloration was possibly present from the nail bed not the fingernail itself, and that the only certain visual change to the fingernail was the surface texture. The white transverse lines seemed to remain in the same locations but faded away over treatment. Onycholysis mostly occurred distally and partially on the sides causing an orange/brown discoloration. This discoloration was also occasionally seen more proximally in the middle in the nail bed but its location remained constant over time. Conditions from literature that resemble these effects include Muehrcke's lines, splinter hemorrhage and subungual hematoma [47]. Muehrcke's lines are composed of white, transverse lines in the nail bed which fade out as pressure is applied, splinter hemorrhage is purple or brown short streaks in the nail bed and subungual hematoma is red or black discolorations in the nail bed [47]. It was observed that the weekly dosed patients had more cases of onycholysis and discoloration as well as larger scaling values for numbness. These findings correlate positively with results from Kibata et al. stating that increased docetaxel administrations were directly related to the degree of nail alterations [58].

During the first half of weekly and biweekly chemotherapy treatments, the median TOF decreased, which could be caused by a less hydrated, denser and/or thinner fingernail. This could be the result of decreased blood flow to the fingernail which may cause disruptions in growth and structure. During the last half of treatment, compared to the measurements at the half-way point, fingernail TOF had increased, possibly showing

a regeneration of growth and increased blood flow, rehydrating and hardening the fingernail. TOF at a specific location is defined in this case as the thickness of the fingernail plate divided by the sound velocity. Sound speed is then defined as the square root of the bulk modulus divided by the density of the fingernail location [39]. This hints that any combination of these four parameters can be changing within the fingernail plate to deviate from the reference TOF measurement. If the TOF first decreases within the first half of a patient's treatment, then it may be possible that the thickness of the fingernail decreases proportionally, the density decreases, or the bulk modulus increases; for an increase in TOF, the opposite effects would occur. A 2009 study by Farran et al. stated that drier (thinner) fingernails are prone to brittle behavior, comparable to the flaking and fragility of patients' fingernails due to onycholysis as observed in this study [59]. A consequence of drier fingernails is a decrease in strain, and hence bulk modulus, and an increase in density, as well as increase in sound speed, due to a decreased nail volume from lower levels of hydration [17]. Putting this all together it is possible that within the first half of treatment some patients developed a drier or thinner fingernail plate, and in the last half the nails began shifting to become wetter or thicker. Of course, other molecular changes may have altered the mechanical structure of the fingernails. There were some unavoidable restrictions in the study, including limited patient volunteers, which provided ranges for variation in gender, age and ethnicity. Most patients undergoing taxane-based treatments were women with breast cancer, and so more men would be required to thoroughly investigate the effects on both genders. In conclusion, this study is the first to investigate the quantitative effects of fingernails as a biomarker of chemotherapy treatment using ultrasound assessment. Based on the outcomes of this preliminary data collection it was validated that there are adverse effects present in the fingernail during chemotherapy treatment, which gave way to obtaining further quantitative data on fingernails to detect changes.

Chapter 3 METHOD FOR FINGERNAIL PROPERTY CHARACTERIZATION BY REFLECTANCE ULTRASOUND TECHNIQUE

Summary: This chapter looks to build on the ideas from the previous chapter but by applying a novel ultrasonic approach with 19 MHz frequency for the calculation of additional acoustic and mechanical properties of fingernails. This method also employs the use of calibration phantoms to ensure that device accuracy is maintained before being applied to human fingernails.

3.1 Determination of Impedance, Density and Elasticity by Simultaneous Measurement of Thickness and Sound Speed

The previous chapter introduces the idea of quantitatively assessing fingernails as a possible biomarker in chemotherapy treatment. This was accomplished with preliminary results considering fingernail plate TOF and its patterns over treatment periods. The outcomes of the prelusive data collection provided confirmation that fingernail defects are present and can be measured. To further investigate the fingernail more in-depth other parameters must be scrutinized. In the search to determine the acoustic and mechanical properties of fingernails, many ultrasonic techniques are available with benefits for different situations. One such method involves using the reflection amplitude on the surface of a sample material in comparison to the surface reflection amplitude on a reference material to distinguish sample material properties. This technique utilizes the longitudinal wave amplitude of a reference and unknown material in pulse-echo mode. By transforming the amplitudes into intensities their division yields the reflection coefficient of the unknown sample [60]:

$$R = \frac{I_{sample}}{I_{ref}} \tag{38}$$

Where I_{sample} is the surface intensity of the unknown sample material and I_{ref} is the surface intensity of the known reference material.

The acoustic impedance of the unknown sample can then be calculated by knowing the acoustic impedance of the coupling layer/liquid (Z_{couple}) by:

$$Z_{sample} = Z_{couple}\frac{1+\sqrt{R}}{1-\sqrt{R}} \tag{39}$$

The density of the unknown sample is then calculated by:

$$\rho_{sample} = \frac{Z_{sample}}{v_{sample}} \tag{40}$$

Where v_{sample} is the sound speed of the unknown material.

Finally, the elasticity or Young's modulus (Y_{sample}) can thus be calculated for an assumed homogenous, isotropic case by:

$$Y_{sample} = \rho_{sample} {v_{sample}}^2 \tag{41}$$

3.1.1 Other Ultrasonic Reflectance Methods and Applications

Other methods include multiple reflection methods, transmission methods and angular reflection methods. A useful technique as written in an article by Hoche et al. uses the multiple reflection echoes from the front and back boundaries of a sample to determine the reflection coefficient of certain liquids [61]. This method is used to calculate the density, acoustic impedance and reflection coefficient based on the TOF and three signal echo reflections from the sample boundaries [61]. The reflection coefficient is calculated by interpreting the amplitudes of the three reflected echoes: A_1 (the first signal echo on the surface), A_2 (the second signal echo from the bottom on the liquid interface) and A_3 (the signal echo that has passed through the liquid twice before reflecting back). Altogether, these amplitude magnitudes can be linked to calculate the reflection coefficient of the sample liquid by [62, 61]:

$$x = \frac{A_1 * A_3}{A_2} \tag{42}$$

$$R = \sqrt{\frac{x}{x-1}} \tag{43}$$

Where x is an arbitrary variable and R is the reflection coefficient.

The density of the liquid can then be calculated with the use of Equation (40) for sound speed from knowledge of the material thickness and calculating the TOF of the liquid and knowledge of the coupling layer acoustic impedance:

$$\rho_{sample} = \frac{Z_{couple}}{c_{sample}} \frac{1+R}{1-R} \tag{44}$$

Where ρ_{sample} is the density of the liquid under investigation, Z_{couple} is the acoustic impedance of the coupling layer and c_{sample} is the sound speed of the sample liquid.

The acoustic impedance of the sample Z_{sample} can then be calculated by:

$$Z_{sample} = c_{sample}\rho_{sample} \tag{45}$$

A second method of determining sample properties via first calculating reflection coefficient can be seen in an article by Chung et al [63]. Here, the ratio of sample amplitude to reference amplitude is considered but in the frequency domain as opposed to the time domain. The reflection coefficient is obtained by resolving the amplitude of the sample material from the front surface in the frequency domain (F_{sample}) and dividing by the amplitude of the reference material also in the frequency domain (F_{ref}):

$$R = \frac{F_{sample}}{F_{ref}} \tag{46}$$

The density and acoustic impedance is then determined in the same fashion as in Equations (40) and (41).

3.1.2 Single Element Focused Transducer Probe, Setup and Software

With a new methodology, different requirements and, feedback from the data collection a revised transducer was to be implemented. A user-friendly, hand-held probe was required with a solid delay line that could be placed directly on top of the fingernail. A high ultrasonic frequency was still required but due to the availability and cost a lower frequency than 50 MHz was used although medical ultrasound frequencies still use the range 1-20 MHz. Since the reflectance method uses a surface reflection and does not penetrate the fingernail structure, a lower frequency was sufficient for this analysis. The ultrasonic probe used for this application was purchased directly online from a manufacturer given a required central frequency. The hand-held probe consisted of a 19 MHz spherically focused, single-element transducer with a 8.9 mm focal distance that was ensured by attachment of a polystyrene cone tip. The frequency bandwidth of the probe was provided as 96% of the central frequency. A spherically focused transducer was used in this application to provide enhanced lateral resolution within the focal zone which in our application would be the surface of the sample object or bottom of the cone tip. The longitudinal wave component only was under measurement in this study due to its higher sensitivity and intensity allowing a clearer signal distinction between cone tip and sample surface in near-normal incident angles. The central frequency was chosen to match frequencies of previous research but also to reduce cost. The shape and size of the probe itself was chosen to give the user a user-friendly grip, similar to a pencil, for ease-of access in viewing and changing location of measurements. The probe was connected to a custom made acquisition board that would be able to connect via USB and to the probe. The board itself as shown in Fig. 3.1 was comprised of a Cypress FX2 universal serial bus (USB) circuit able to receive 5V and 500mA from a source such as a laptop, a power management circuit to organize how the power was distributed throughout the circuit, an Altera Cyclon IV field programmable gate array (FPGA) circuit, a pulser and a 12 bit analog to digital converter (ADC) circuit.

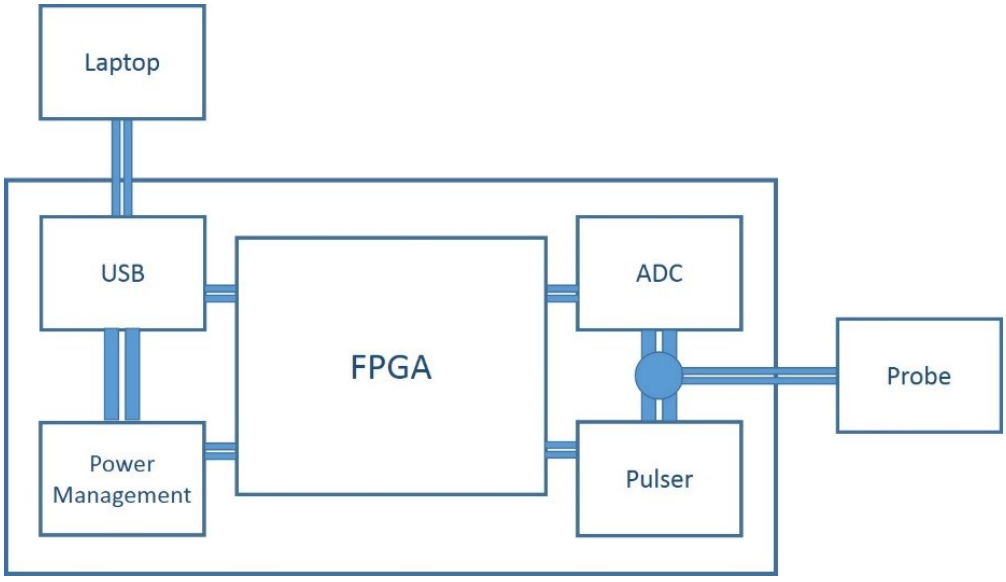

Figure 3.1: Diagram of acquisition board components and their external connections. The board itself is composed of a USB circuit, power managements unit, FPGA, ADC and pulser which is connected to the probe at one end and a laptop on the other end.

The software coding used for this application was accomplished using MathWorks Inc., MatLab R2012a software. The software enabled the user to obtain A-scans at different locations on the sample by controlling the duration time of pulsing and how the output was displayed. For this application, the Peak-to-Peak amplitude of the signal was considered as to accurately distinguish the maximum amplitude from noise or power spikes.

3.1.3 Calculations for Thickness and Sound Speed Determination

Assuming that the thickness of a sample and the sound speed is unknown, then certain approaches must be taken in order to determine these crucial parameters. Two methods will be considered in this thesis to determine the thickness of a sample; one using OCT and the other using ultrasound. An OCT scan uses reflected backscattered light from a material's microstructure to produce a high resolution image on the scale of microns [64]. It provides a cross-sectional image (B-scan) on the basis of multiple A-scans from time-delayed signals similar to ultrasound but using light as opposed to sound and with much better resolution. This method is beneficial for its high resolution and

non-invasive, real-time imaging but its downside its high scattering and attenuation through tissue limiting its penetration depth to about 2 mm only [64].

The second method of thickness measurement employs the use of ultrasound to detect the maximum amplitude at each of the interface boundaries of the sample under investigation. This method is also known as the V(z) method or double/variable focus technique [27, 65, 66]. It involves using a focused ultrasonic beam and focusing the focal spot on the first interface then shifting the position of the transducer by a known amount to focus on each subsequent interface boundary [27]. By knowledge of the displacement of the transducer, one can determine the thickness of each of the layers present evident every time the amplitude reaches a local maximum. This method is resolved to the accuracy of the motor that performs the displacement and its incremented steps of displacement.

Both of the above approaches can be then used to determine the sound speed of the sample alongside finding the TOF between the layers. The TOF can be determined with a single ultrasonic A-scan of the sample. The A-scan will contain a series of local maximum peaks which are deemed to be the boundary interfaces. Most likely the difference between them will be assigned in number of samples taken which must then be converted to time by considering the sampling frequency. The sampling frequency is related to the sampling rate and the amount of supersampling by:

$$f_{sampling} = \frac{SS}{SR} \tag{47}$$

Where $f_{sampling}$ is the sampling frequency (s^{-1}), SS is the amount of samples supersampled and SR is the sampling rate (s).

Then the TOF is determined by the number of samples between interfaces and the sampling frequency by:

$$TOF = \frac{samples}{f_{sampling}} \tag{48}$$

Thus the sound speed is finally determined by dividing the thickness of the layer by the TOF determined for that layer.

3.1.4 Calculations for Impedance, Density and Elasticity Based on Reflectance Amplitude of Sound Waves

In order to calculate the acoustic impedance, density and elasticity of an unknown sample the reflection coefficient must be calculated in the same manner as Equations (38)-(41). In this thesis, the method of reference and sample intensity ratios from surface reflection amplitudes will be used to determine the reflection coefficient. The other methods mentioned were tested as well but they did not prove to be as accurate and repeatable as this method. By considering the known parameters of the reference and sample a simplified equation was created for the reflection coefficient based on the maximum amplitude of the reference (A_{ref}), and the unknown sample (A_{sample}).

$$R = \frac{{A_{sample}}^2}{{A_{ref}}^2 (reflection\ loss)} \tag{49}$$

The reflection loss factor was calculated based on the known impedance of the coupling medium Z_{couple} and reference material Z_{ref} to calculate the transmission and compensate for it.

$$reflection\ loss = 1 + \left[1 - \left(\frac{Z_{ref} - Z_{couple}}{Z_{ref} + Z_{couple}}\right)^2\right] \tag{50}$$

From this point the impedance, density and elasticity are calculated the same as in Equations (40)-(41) using the sound speed calculated by the methods in the last section.

3.1.5 Expected Results from Healthy Fingernail Measurements

Based on literature values, fingernail thickness can range from 0.3-1 mm with an average thickness of 0.49±0.15 mm and a growth rate of 3.47 mm/month [16, 67]. The sound speed of fingernails was confirmed to be in the range of 1650-2760 m/s with an average of 2470 m/s [28, 29]. The density of healthy fingernails was calculated by a group of researches using pycnometry and determined to be 1.34 g/cm^3 at room

temperature with 40-60% relative humidity which is the normal humidity range that human fingernails are exposed to [67]. Another study by Farran et al. was conducted on 50 healthy fingernail clipping and was found that at 55% relative humidity the Young's modulus was stated to be 2.32 GPa [59]. A different study showed a wider range of elasticity values for both male and female fingernails with fingernail thicknesses ranging from 0.29-0.44 mm and elasticity values ranging from 3.5-5.5 $x10^{10}$ dynes/cm^2 [68]. Minimal studies have been performed in regards to these parameters accurately calculated and so these reference literature values are to be taken as a guide for comparison since many factors can contribute to changes in these values.

Chapter 4 EXPERIMENTAL PROCEDURE

Summary: This chapter aims to outline the need for calibration phantoms as well as explanation of the procedure leading to fingernail measurement.

4.1 Calibration and Accuracy Assessment

Continuing from the previous chapter, the method of ultrasound reflectance requires the use of a reference material with known properties. For this reason, pure metals were chosen which possessed properties that could be identified in literature. Not only are the calibration phantoms used as a reference, they also allow the calculation of device accuracy and repeatability. Due to the fact that these materials are assumed pure, isotropic and homogenous they are ideal candidates to use. The term phantom in this thesis refers to materials that are used to evaluate the effectiveness of an imaging modality or device. One main goal of this thesis was to determine the characteristic properties of fingernails with as much accuracy as possible. As a way to confirm our accuracy these calibration materials were used to assess our procedure's level of accuracy before applying it on fingernails. Fingernails possess many layers of keratinized structure with differing hydration and density properties therefore an objective was to ensure data had greatest signal-to-noise and minimal variation. To accomplish this, four metals (Fig. 4.1) were used as our initial calibration phantoms: pure rolled zinc, pure rolled copper, pure rolled aluminum and 1018 stainless steel. The exact chemical compositions of these metals were not available from the manufacturer although they stated it as being pure. They were assumed to be pure and were searched in literature as such. Before testing, the four metals were polished flat several microns to ensure no surface defects were present.

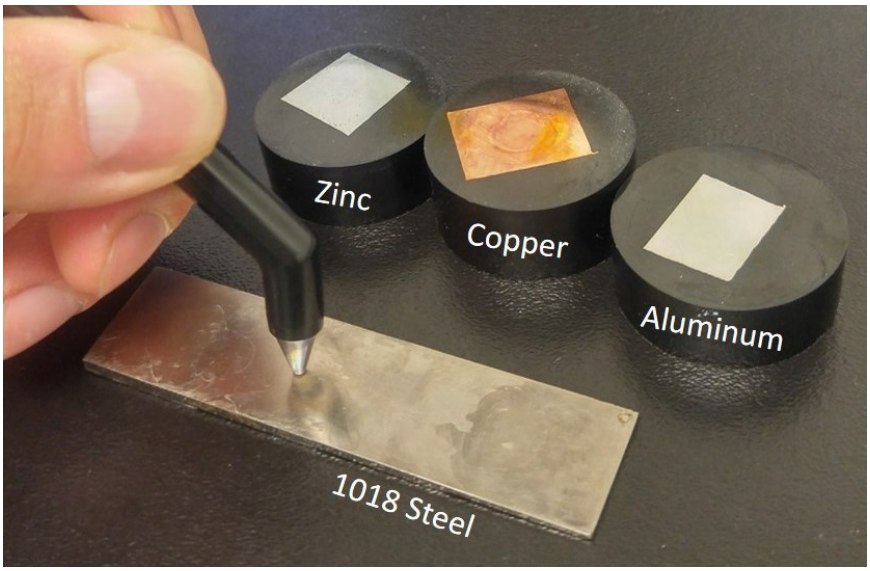

Figure 4.1: Diagram showing probe to measure the four metal phantom blocks: pure zinc, pure copper, pure aluminum and 1018 steel.

The metals were chosen due to their availability and their high impedance values allowing maximum reflection between them and the coupling material polystyrene on the tip of the transducer. They were also chosen due to them being a homogenous, isotropic and pure material that would ideally have almost identical values throughout their bulk volume. The key to their ability as being calibration materials was their consistency in values as was proven in the next section. The literature values of each of these types of metals are provided in Table 4.1. The density, impedance and sound speed are purely based on other articles and the elasticity was calculated using Equation (45) to keep the methods consistent throughout this thesis. Elasticity values calculated may differ from ones in literature, possibly due to their different composition of the metals not exactly specified and the different equations used which were not always outlined in the literature.

Table 4.1: Material phantom types and their literature values.

	Material Type [69,70]			
	Copper	**Zinc**	**Aluminum**	**1018 Steel**
Density (g/ cm^3)	8.90	7.10	2.70	7.80
Impedance (MRayl)	41.8	29.6	17.1	46.1
Sound speed (m/s)	4660	4170	6374	5917
Young's modulus (GPa)	193	123	110	273

The thickness and TOF of the metals were able to be measured to ensure the sound speed was in close proximity to that of the literature values. The thickness was measured using a micrometer 10 times then averaged, and the TOF was measured using a 50 MHz ultrasound probe 10 times and also averaged. The difference between the literature values and the calculated sound speed are given in Table 4.2. The percent difference between the literature and calculated values were all smaller than 3% for the highest deviations considered.

Table 4.2: Difference between literature values and calculated values for sound speed in each of the four metal phantoms.

	Calculated (m/s)	**Literature (m/s)**	**Percent Difference**	**Coefficient of Variation**
Copper	4723±53	4660	2%	1.0%
Zinc	4133±30	4170	2%	0.7%
Aluminum	6380±53	6374	1%	0.8%
1018 Steel	5835±53	5917	2%	0.9%

To test which of the phantoms would provide the most accurate values based on our reflectance method compared to literature values, each of them were used as the reference while the remaining were set as the samples to be identified. The single metal phantom that showed the most accurate resemblance to the literature was then used to reference and calculate the properties of a fingernail sample *in-vivo*. This was based on the sound speed values used from Table 4.2 and the amplitude obtained for each single measurement. For statistical purposes, 10 measurements of each metal used as a reference were taken to establish which of them was best suited to be most accurate before being applied to fingernail measurements.

4.2 Fingernail Measurement Procedure

Once a reference material was identified its maximum surface amplitude was obtained for use in calculation. This was accomplished by setting a timer on the program code in order to collect enough data to give the best representation of the maximum amplitude; this would be difficult since the probe head was very sensitive to angular movement. A timer was set to one minute to allow the user to manipulate the probe head until the maximum was clearly obtained on the live A-scan display. The maximum reference amplitude was recorded at the end of the minute and the program provided the calculated parameters based on the sound speed and amplitude obtained. The remaining step was to obtain the maximum amplitude of the fingernail at a desired location. The probe was placed on top of the fingernail closest to the center and the program was run for one minute. The user handled the probe as to obtain the optimal angulation for maximum amplitude registration. In conjunction with the fingernail amplitude the sound speed of the fingernail was combined to the code based on either the OCT or ultrasound thickness measurements. With these three values the impedance, density and elasticity of the fingernail was determined. This procedure was conducted 10 times on the fingernail for statistical purposes and an average value was deduced for each parameter calculated.

Chapter 5 EXPERIMENTAL RESULTS AND DISCUSSION

Summary: This chapter intends to first validate the accuracy and repeatability of the 19 MHz ultrasonic probe using calibration phantoms then determine the acoustic and mechanical properties of a fingernail in-vivo.

5.1 Assessment of Fingernail Thickness, Sound Speed, Impedance, Density and Elasticity

5.1.1 Accuracy of Transducer Based on Known Calibration Materials

As mentioned in Section 4.1, each of the metal phantoms were tested as the reference to identify which gave the closest values to that of literature. For each case, a total of 10 measurements of the Peak-to-Peak amplitude were recorded and averaged. The impedance, density and elasticity were then based solely on the reference metal amplitude, sample metal amplitude, and sample sound speed. It was proven that 1018 steel was the best candidate as the reference material due to the fact that it had the lowest percent difference between experimental values and literature values as shown in Table 5.1-5.3 for all parameters tested. The error for each calculated value was obtained using the standard deviation as opposed to standard error to allow a greater error discrepancy for a more realistic deviation. The percent difference was calculated based on the experimental values calculated and the expected literature values. The coefficient of variation was also calculated based on the experimental value and its associated error.

Table 5.1: Experimental and literature values obtained for aluminum with 1018 steel reference based on 10 measurements.

Aluminum				
	Experiment	Literature	Percent Difference	Coefficient of Variation
Reflectivity	0.6±0.1			
Sound speed (m/s)	6380±53	6374	1%	0.8%
Impedance (MRayl)	18.7±0.2	17.1	9%	1%
Density (g/cm^3)	2.93±0.02	2.70	8%	0.7%
Elasticity (GPa)	119.27±0.01	109	8%	0.01%

Table 5.2: Experimental and literature values obtained for copper with 1018 steel reference based on 10 measurements.

Copper				
	Experiment	Literature	Percent Difference	Coefficient of Variation
Reflectivity	0.8±0.1			
Sound speed (m/s)	4723±20	4660	1%	0.4%
Impedance (MRayl)	46.5±0.2	41.8	10%	0.4%
Density (g/cm^3)	9.85±0.01	8.90	10%	0.1%
Elasticity (GPa)	219.65±0.01	193	12%	0.01%

Table 5.3: Experimental and literature values obtained for zinc with 1018 steel reference based on 10 measurements.

Zinc				
	Experiment	Literature	Percent Difference	Coefficient of Variation
Reflectivity	0.8±0.1			
Sound speed (m/s)	4133±30	4170	1%	0.7%
Impedance (MRayl)	35.4±0.2	29.6	16%	0.6%
Density (g/cm^3)	8.56±0.01	7.10	17%	0.1%
Elasticity (GPa)	146.25±0.01	124	15%	0.01%

Based on 1018 steel being the reference material, the highest percent difference between experiment and literature was determined to be 17%, as seen in the zinc block. The material with the lowest percent difference was determined to be aluminum with a minimum of 8%. The material with the highest coefficient of variation was found to be aluminum, and the material with lowest values for coefficient of variation was determined to be copper. These very low variations are likely caused by the fact that the metals were polished to remove any sort of imperfections or granularity on the surface as well as make them as flat as possible to make it easier to maintain the probe tip perpendicular to the surface.

5.1.2 Repeatability of Measurements

The comparison of each material to one another in terms of accuracy was accomplished in the previous section, but the repeatability of each metal individually was also to be investigated. Each of the four metal phantoms were subject to repeatability tests to observe how much the amplitude would deviate based on 10 measurements in different locations. The results are displayed in Table 5.4.

Table 5.4: Repeatability differences of all four metal phantoms used for calibration.

	Average Amplitude	Standard Deviation	Coefficient of Variation
1018 Steel	15817	±98	0.6%
Aluminum	13422	±405	3.0%
Copper	15568	±143	0.9%
Zinc	15090	±363	2.0%

The maximum coefficient of variation between repeated measurements was 3% for different locations which was within a 95% confidence interval. This analysis was very important because the error of probe must be as small as possible to validate that the results are real and not due to noise or random fluctuations. This could have major impacts on the calculated values since certain equations require exponential products causing a small change in value to become much different than anticipated. The amplitude obtained was very sensitive to angulation changes therefore this is a major cause of the error since the materials themselves are thoroughly uniform.

5.1.3 Sound Speed Measurements of Fingernail

One of the input parameters required to calculate the reflection coefficient using the reflectivity method is the sound speed of the material under investigation. Two methods were tested in order to assess the thickness and sound speed of a fingernail using ultrasound and OCT. Both of these methods were considered and compared to observe their usefulness. A single image on an OCT machine was taken of a thumb fingernail *in-vivo* of a 29-year old healthy male in the sagittal plane (Fig. 5.1) and the thickness across that portion was averaged to an accuracy of 0.005 mm. The average thickness was found to be 0.57 mm according to the software equipped on the OCT machine.

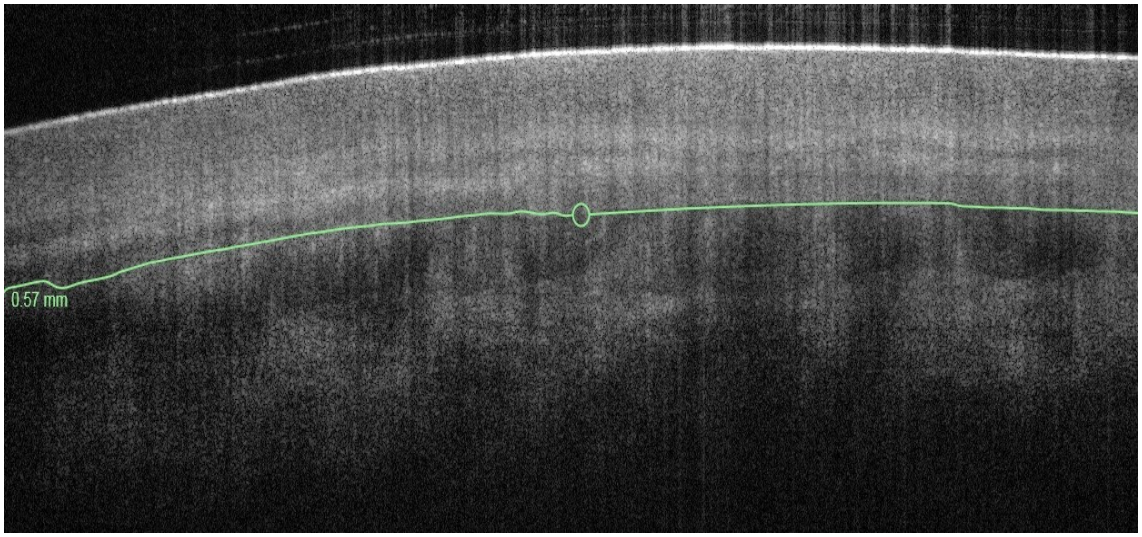

Figure 5.1: OCT image measuring the average thickness of an in-vivo fingernail. The green line represents the bottom interface of the fingernail as identified by the OCT software. The value on the left is the average thickness along the green line.

The thickness of that same fingernail was then determined using the ultrasonic V(z) approach which identified the translated displacement required to obtain maximum amplitude reflections from the top and bottom interface of the fingernail plate. This was performed using a scanning acoustic microscope developed by Tessonics Inc., Windsor, CA connected to a 50 MHz transducer with a 7 mm focal length – the same as used in the data collection (Fig. 5.2). The accuracy of the moving motor attached to the transducer limited the incremented displacement by 50.8 μm. Based on the number of samples between the maximum amplitude of the two interface boundaries the thickness of the fingernail was found to be 0.51±0.05 mm. This corresponded to a difference between OCT and ultrasound methods of 11%. This difference may be due to the fact that the two methods were not performed in the exact same location and so different spots of the fingernail may fluctuate in thickness. The TOF of the fingernail was then determined by a single A-scan to measure the amount of samples between the two local maximum peaks identified as the fingernail plate (Fig. 5.3).

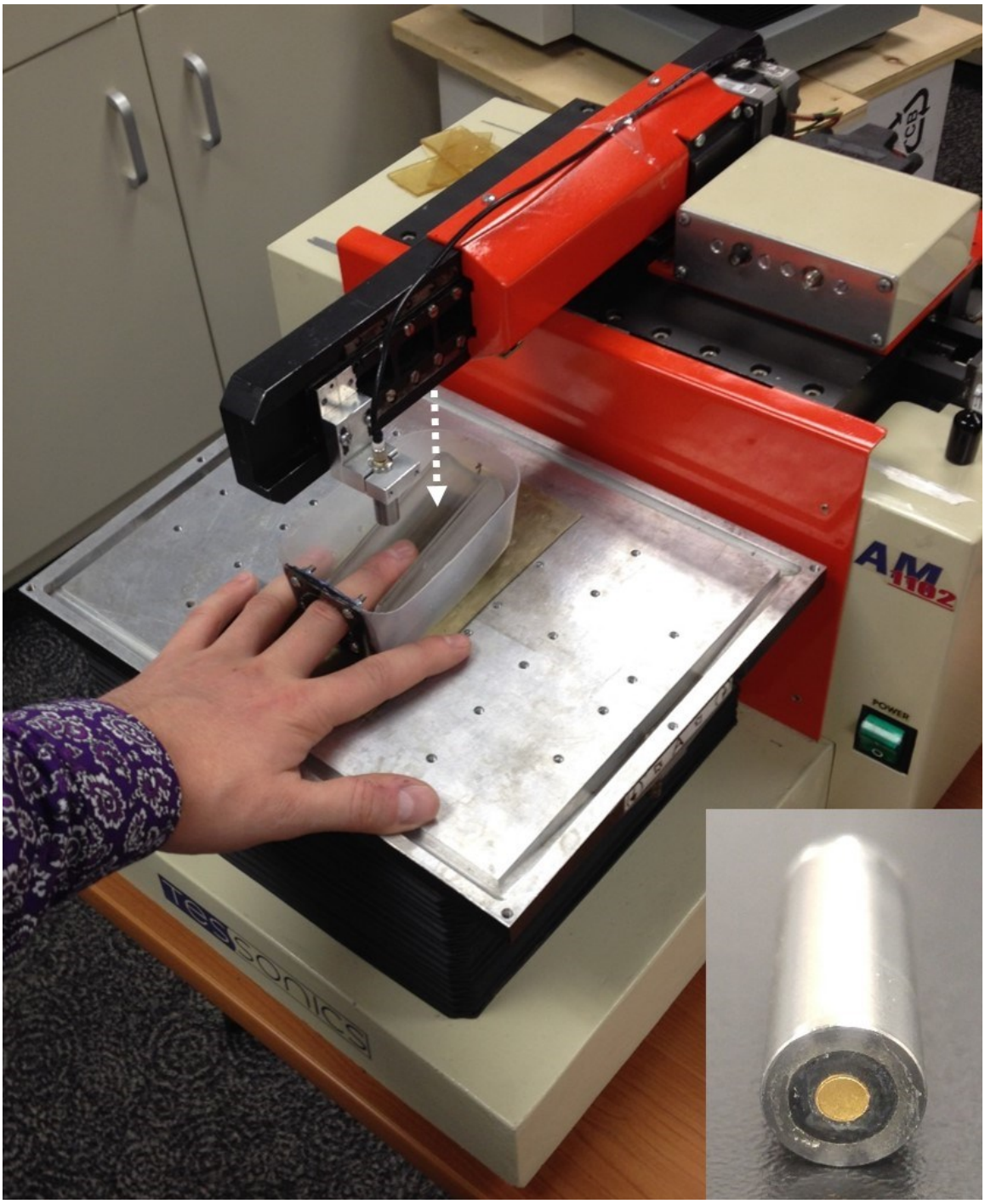

Figure 5.2: Setup used to obtain the thickness of fingernail using ultrasound in V(z) mode. The dashed arrow indicates the direction of motion on the transducer. The bottom right image shows the transducer where the gold circular area is the aperture surface.

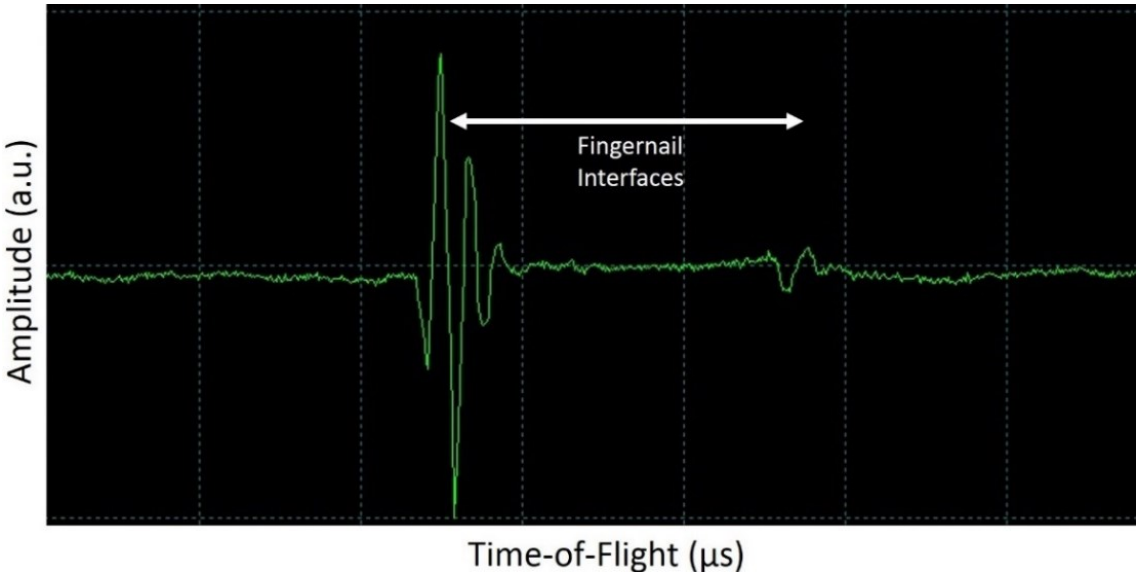

Figure 5.3: Diagram of a single A-scan from an in-vivo fingernail showing the interface boundaries identified by the separated amplitude peaks.

With the two different thicknesses from the OCT and ultrasound method and the single value of TOF two different sound speeds were determined for each method (Table 5.5). The OCT measurement corresponded to a fingernail sound speed of 2487.45±0.01 m/s and the ultrasound measurement corresponded to a fingernail sound speed of 2225.6±0.1 m/s. Both of these values are well within the range of fingernail sound speed values determined by several articles [17, 28, 29]. A source of error includes measurement locations being more proximal or distal causing small deviation in sound speed. Additionally, different time periods of measurement might cause changes due to diet and humidity of the fingernail but it is unknown how significant these changes may or may not be. Due to the low availability of the OCT machine only a single measurement on one fingernail was possible.

Table 5.5: Sound speed values for OCT and ultrasound methods used to calculate fingernail thickness at a single location.

	Thickness (mm)	**TOF (µs)**	**Sound Speed (m/s)**
OCT	0.570±0.005	$4.58\text{x}10^{-7}\pm5\text{x}10^{-9}$	2487.45±0.01
Ultrasound	0.51±0.05		2225.6±0.1

5.1.4 Impedance, Density and Elasticity of Fingernail

As per previous examples of calculations the impedance, density and elasticity of the fingernail under example can be determined with knowledge of the maximum surface signal amplitude and sound speed. The results obtained from calculation for the 29 year-old male fingernail are provided in Table 5.6. For this data, the sound speed based on the OCT thickness of the fingernail was used due to its greater accuracy of error. The impedance of fingernails was not found in any literature and so the literature values were calculated using the literature sound speed and density. As performed before, the elasticity was calculated using Equation (42). The literature elasticity, or Young's modulus mentioned before in Section 3.1.5, was different than that of the one written in Table 5.6 possibly because the fingernails used in that study did not include the thumb which is the thickest of all fingernails. The thumb fingernail may possess increased rigidity and stiffness as well as the thickness of fingernails in literature were much less than the one obtained from our volunteer. The largest percent difference obtained for the fingernail measurement compared to literature was 16% which was within the limit for the calibration phantoms of 17%. Although the comparison to literature was sufficient, the coefficient of variation was much larger in the fingernail sample than in the metal phantoms. This was to be expected since the phantoms purpose was to ideally have perfectly uniform and isotropic surfaces while fingernails contain a rough and anisotropic surface.

Table 5.6: Experimental fingernail properties on the thumb of a 29-year old male and the associated literature values for a wide range of volunteer demographics.

Male Thumb Fingernail				
	Experiment	Literature	Percent Difference	Coefficient of Variation
Reflectivity	0.1±0.1			
Sound speed (m/s)	2487.45 ±0.01	2470 [29]	1%	0.01%
Impedance (MRayl)	4±2	3.3	15%	50%
Density (g/cm^3)	1.6±0.5	1.34 [67]	16%	31%
Elasticity (GPa)	9.8±0.3	8.2	16%	3%

5.1.5 Reflectivity Curves

Considering a more general approach to viewing the data, distribution curves were created to illustrate the effect of reflectivity of a material on the impedance, density and elasticity. By encompassing the entire reflectivity range from 0-100%, the impedance was calculated accordingly. The reflectivity for each unit of impedance up to 100 MRayl - which most metals are included under - is shown in Fig. 5.4. There are many alloys of the metals used in this study and Fig. 5.5 provides a representation of the change in density for the materials based on their reflectivity in extreme cases. Similarly, elasticity values for the entire range of possible reflectivity is shown in Fig. 5.6 in extreme cases. In general, as a pattern based on the three graphs, it was observed that the lower the reflectivity a material had the lower the impedance, density and elasticity it has accordingly. All of these graphs were created using the equations provided in this thesis and should only be referenced if the same equations are used. No equation of best fit was able to be calculated for any of the below graphs.

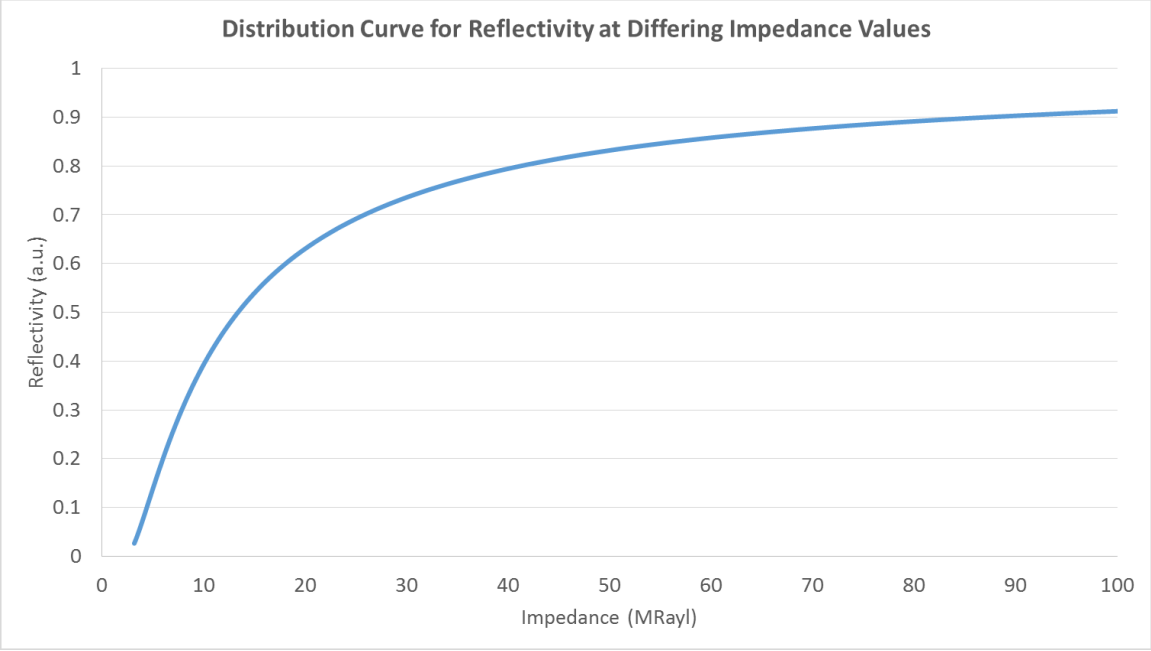

Figure 5.4: Distribution curve for reflectivity at differing impedance values.

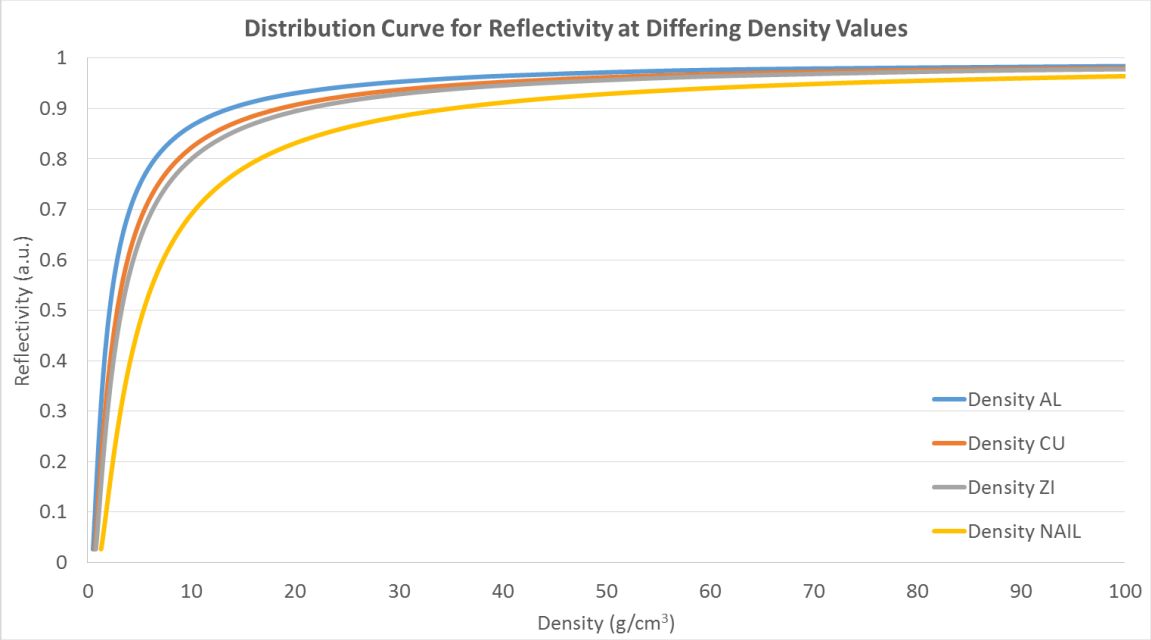

Figure 5.5: Distribution curve for reflectivity at differing density values for aluminum, copper, zinc and the fingernail of a 29 year-old volunteer.

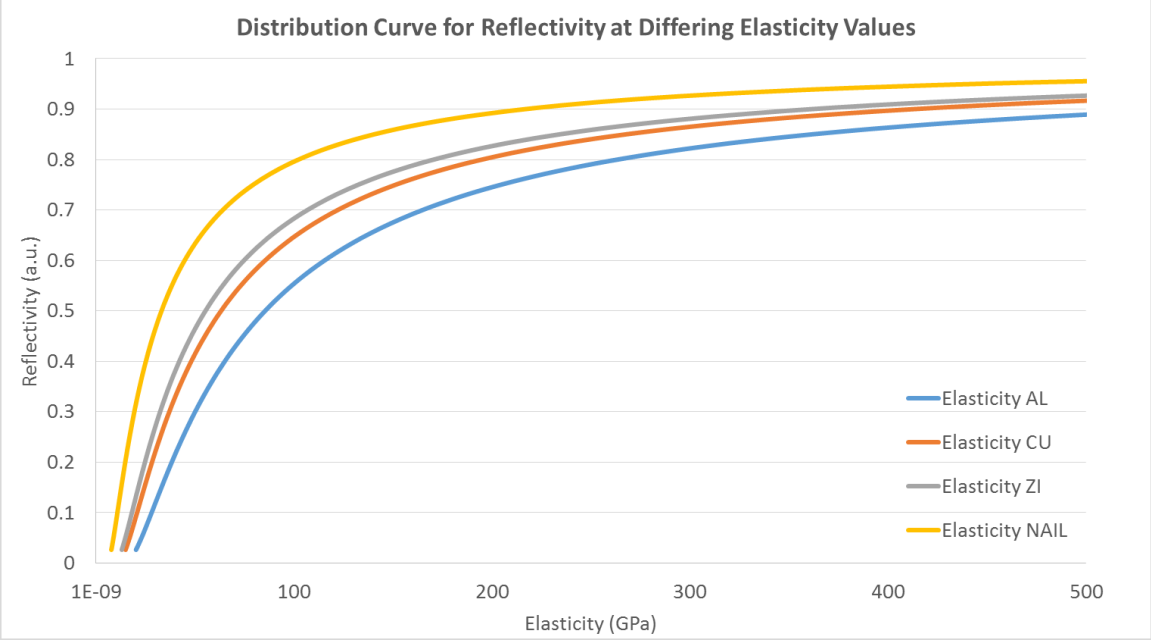

Figure 5.6: Distribution curve for reflectivity at differing elasticity values for aluminum, copper, zinc and the fingernail of a 29 year-old volunteer.

5.1.6 Transducer Probe Resolution

Similar to the transducer in the data collection, the resolution for the hand-held probe was determined to assess its acoustic parameters for future reference. The lateral resolution of the probe was simply determined by the diameter of the polystyrene cone tip since at this spot the focal point is located. The diameter of the cone tip measured by calipers was determined to be 2.00±0.05 mm. The axial resolution was determined similar to that of the previous transducer by measuring the FWHM pulse width at -6 dB of the signal. A pinducer was placed very close to the tip of the transducer cone while all submerged in water in the same manner as before. The pinducer acted to receive the transmitted signal from the closest point to cone tip focal spot. The recorded pulse was then considered based on its pulse length to measure its resolution along the axial direction. The pulse length was measured in units of time (Fig. 5.7) and then converted to distance by the use of the sound speed of the propagation medium polystyrene (2350 m/s) [69]. The pulse length was at first expressed in normalized units of intensity then integrated over the entire pulse time (Equation (24)) to calculate the pressure exerted. The pulse length was determined to be $3.0\text{x}10^{-7}\pm0.3\text{x}10^{-7}$ s long in polystyrene. Thus, the axial resolution of the surface pulse was calculated to be 0.26±0.03 mm.

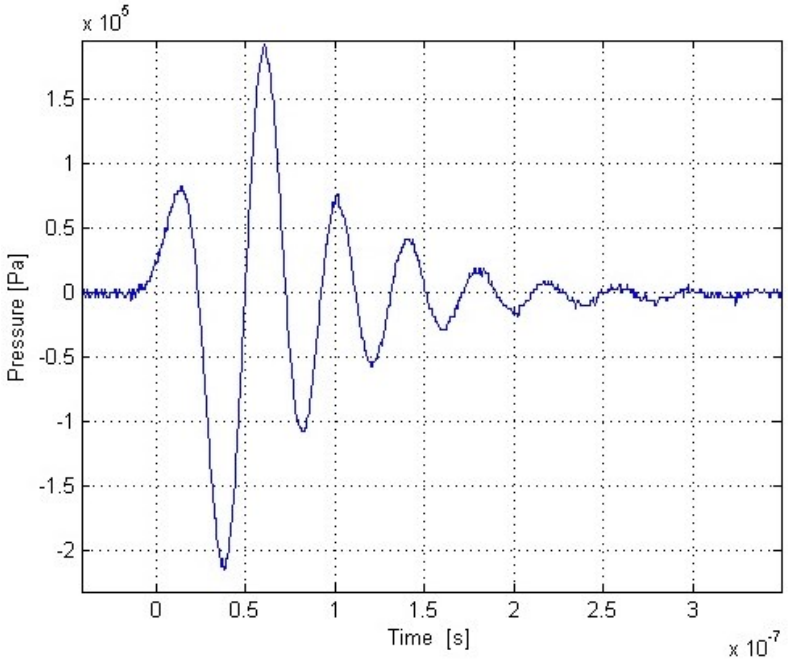

Figure 5.7: Acoustic pressure pulse of single incident wave from 19 MHz probe on pinducer as a function of time.

5.2 Discussion

In Chapter 2, a clinical data collection was described as a proof-of-concept to observe qualitative and quantitative changes to fingernails on patients being administered chemotherapy. By the end of treatment patients complained about doing up buttons and opening bottle caps as well as lifting heavier objects compared to pre-treatment examination. The most common visual deformity of the patient group was firstly onycholysis, seen as nail detachment and/or discoloration, and secondly as white transverse lines and/or white lunula. Onycholysis was likely to have been caused by mitotic cessation and cell death as a slow process over the course of treatment. Each white transverse line was likely associated with a treatment session where the body was suddenly toxified with taxane and regeneration or survival of cells in that short period was greatly reduced causing a white band. The observations made during this study have been validated in the past stating that chemotherapy, and specifically Paclitaxel, does induce fingernail alterations such as darker pigmentations and onycholysis [70, 71]. Although a frequently cited paper found that 41% of patients develop nail changes from Docetaxel and only less than 2% develop defects from Paclitaxel, the cases in this study differ seeing as there was a combination of chemotherapeutic drugs administered, not solely Paclitaxel [72]. Comparisons between the results of this study and those of other studies would generally not follow as effects may be compounded [70].

Based on the ultrasound measurements of TOF for all 17 patients, it was identified that within the first half of taxane chemotherapy treatment 50% weekly and 100% biweekly dosed patients demonstrated to have a decrease in the median TOF. In the last half of treatment, for 86% weekly and 88% biweekly dosed patients it was demonstrated that there was an increase in median TOF. Lastly, comparing the beginning to the end of treatment, it was observed that 75% weekly and 50% biweekly dosed patients were measured to have an overall increase in median TOF. As mentioned previously, this pattern of changes could have been due to the degeneration then regeneration of fingernail nutrient blood supply which caused alterations in the density, hydration and thickness of the fingernail. This study validated the use of ultrasound to qualitatively determine preliminary diseased fingernail characteristics over the course of a cancer

treatment. Further investigation is required to supply more information about the fingernail hence a new method of approach was developed using ultrasound reflectance to further identify fingernail parameters.

The method of ultrasound reflectance was then implemented in Chapter 4. A different transducer and setup was also used for this alternate technique. A lower frequency - 19 MHz - compared to the previous 50 MHz was utilized due to several reasons. Due to the fact that only the surface amplitude was required and no depth penetration was necessary then it was enough to use a lower frequency transducer which was less costly and could be purchased in a smaller, user-friendly and hand-held probe design with a solid delay line that would sit directly on top of the fingernail. To note, diagnostic ultrasound probes currently work in the regime of 1-20 MHz and so, 19 MHz was still considered a high frequency for tissue testing. Although the frequency of transducer was reduced to 19 MHz, the lateral resolution was very similar with both. The 50 MHz transducer had a lateral resolution of 2.1±0.1 mm and the 19 MHz transducer had a lateral resolution of 2.00±0.05 mm. The axial resolution of the 50 MHz transducer was determined to be 0.08±0.01 mm and that of the 19 MHz probe to be 0.26±0.03 mm based on their pulse widths. The 50 MHz probe had resolution several times greater than that of the 19 MHz but the 19 MHz probe was still on the order of magnitude to fingernail thickness. This means that if needed the fingernail plate TOF could also be obtained with the 19 MHz probe.

By trial-and-error, it was determined that 1018 steel was the best candidate phantom to be used as the reference material to calculate reflectance. The phantom with the largest percent difference compared to literature was zinc (17%) and the lowest coefficient of variation was for aluminum (1%). The phantom with the smallest percent difference compared to literature was aluminum (8%). The maximum percent difference of zinc may seem relatively high even though the coefficients of variation for each of the phantoms are very low. This can be explained by the high error for the reflectivity thus, all of the preceding values are affected. Also, the exact composition of the phantoms and those in literature are not 100% certain so there may be an error associated with these as well.

In Section 5.1.3, a test trial was performed on a 29 year-old male volunteer's thumb fingernail. Beforehand though, the sound speed of the fingernail was required. Based on the method of either OCT or ultrasound it was concluded that OCT was more accurate thus the fingernail sound speed of 2487.45±0.01 m/s was utilized in further calculations. This value was within the range of fingernail sound speed confirmed by literature. Due to the very low availability of the OCT machine only one single fingernail measurement was possible at the time. Henceforth, the maximum percent difference between all parameters including impedance, density and elasticity compared to literature was in the range of 16% for the fingernail. This was within the maximum percent difference for the calibration phantoms which confirmed the accuracy and precision of the devised technique in a real-life application. Again, the literature values obtained for fingernails were based on many factors including race, age, diet, environment so the reference literature was used as a general guide to ensure the functionality of the proposed device and methodology. The coefficients of variation were much greater for the fingernail than of the phantoms mainly due to the fact that the reflectivity error was on the magnitude of the reflectivity itself causing very large error in the other parameters calculated. Although the errors were large it was expected because compared to the polished, smooth and uniform phantoms the fingernail possessed a very rough and uneven surface which may lead to increased diffraction changing the amplitudes of the received sound waves enough to cause deviations in reflection accuracy. In addition, performing repeated measurements on the same location was challenging.

It must be noted again that the equations used in this thesis are based on the assumption that the transducer was angled directly perpendicular to the sample surface, and that materials were isotropic and homogenous for the most part. Of course, other aberrations are likely present in the fingernail such as scatter but due to the fact that only the surface amplitude of reflection was considered for assumed flat surfaces these effects can be considered negligible. Limitations in the reflectance mode experiment include ensuring the transducer was perpendicular to the surface being measured, using a reference material with known exact specifications and determining the sound speed of the sample being measured accurately at a chosen location. Improvements that could be applied for future investigation could be obtaining a large volunteer group of different

genders, races, ages and with specific fingernail or sub-ungual deformities such as fungal infections to create a database of values. Another improvement would be to create a novel tip on the transducer probe so that the angle of positioning is easier and quicker to achieve an orientation perpendicular to the fingernail plate. The probe itself is miniaturized to an optimal degree but the controller board hardware can be further reduced in size to possibly even fit in a user's pocket for easy transportation.

Chapter 6 CONCLUSION

6.1 Concluding Remarks

Despite the widespread use of diagnostic ultrasound in medicine, little research has been conducted regarding the applications of high frequency ultrasound to oncology, in particular, using the ultrasonic parameters of fingernails as biomarkers of systemic health. The fingernail plate begins its growth from the underlying tissue of the finger called the nail bed and matrix. These tissues are comprised of very rapidly replicating cells that are readily affected by changes to the blood supply provided to them. As the blood composition changes, the nail bed and matrix experience transformations which yield alterations during formation of the fingernail plate. It is well-known that chemotherapeutic agents, especially taxanes, induce adverse effects on the formation of fingernails. One of the aims of this thesis was to investigate whether fingernail plate changes could be assessed by surveying patients undergoing taxane therapy. A second goal of this thesis was to develop and implement an ultrasonic method of measuring and calculating additional acoustic and mechanical properties of fingernails.

Firstly, a clinical data collection was performed on patients receiving taxane regimens to view the changes in fingernail plate TOF and any associated patterns. This study was approved by both the University of Windsor and the Metropolitan Hospital ethics board. A total of 17 patients (16 female, 1 male) participated in this study, with ages ranging from 35-69 years. Measurements of the patient group were performed before treatment, in the middle of a treatment plan, and on the last day of treatment. For this study a 50 MHz ultrasonic transducer operating in pulse-echo mode was used. Similar studies performed previously used transducers with lower frequencies than 50 MHz; it was in our interest to use a higher frequency in effort to acquire improved resolution images of microstructure from B-scans. The transducer resolution and other characteristics are outlined in Section 1.2. A custom, 3D-printed carcass was created for the transducer and a linear stepper motor was connected to allow the movement of the transducer once placed on the surface of a fingernail. For this preliminary trial, only the

TOF from B-scans was to be analysed since the thickness and sound speed in fingernails varies based on position as reported in literature.

The qualitative and quantitative results for the data collection are presented in Section 2.4. It was determined that 47% of patients developed onycholysis and/or discoloration and 24% developed white transverse lines and/or white lunula. In addition, numbness and grip worsened for almost all patients over the course of treatment. By the end of treatment, most patients experienced evident changes in fingertip numbness which was more severe than their grip ability at that same time period. Patients aged over 50 years experienced greater severity of both grip strength and fingertip numbness than did the rest of the participants. Based on the TOF data, it was concluded that 50% of the weekly dosed and 100% of the biweekly dosed patients' fingernails presented with a decrease in median TOF for the first half of treatments. During the last half of treatments, the median TOF was seen to increase for 86% of the weekly dosed and 88% of the biweekly dosed patients. Lastly, when comparing the baseline to end measurements, it was determined that there was an observed increase in median TOF for 75% of the weekly dosed and 50% of the biweekly dosed patients. A decrease in TOF was hypothesized to be caused by a drier, denser or thinner fingernail, while an increase in TOF could be caused by a wetter, less dense or thicker fingernail. The fact that overall fingernail TOF returned to near baseline values may also indicate the onset of cellular homeostasis, whereby the body, and hence the nail bed and matrix cells, adapt to the presence of chemotherapeutic agents and begin repairing damaged pathways. This clinical data collection was the first of its kind, and provided introductory evidence that fingernails serve as possible biomarkers for systemic health during chemotherapy treatment by means of quantitative ultrasonic assessment. It must be recognized that TOF provides only preliminary information as a first step towards validating the hypothesis.

After successfully completing the proof-of-concept data collection, further development of the methodology and procedure was implemented. This included both updated hardware and software. The 50 MHz transducer was replaced with a 19 MHz hand-held probe to create a more realistic scenario in a hospital environment while still providing effective resolution and accuracy. Due to the fact that only the surface reflection was required from the transducer, depth penetration was not an issue, and so a

more economic but equally as effective option was to use a lower frequency alternative still within the high frequency diagnostic ultrasound range. The resolution of the 19 MHz probe was outlined in Section 5.1.6. Along with an alternate transducer, a new method was implemented using ultrasound reflectivity. Several different reflectivity approaches were tested, but the most effective in terms of consistency and accuracy was that using the surface amplitude reflection of a reference material and comparing it to the surface amplitude reflection of an unknown material, all in the time-domain. The equations used and methodology of this process was presented in Chapter 3.

Using the method of ultrasound reflectivity, parameters assessed included acoustic impedance, density and elasticity, employing known calibration phantoms including copper, zinc, aluminum and 1018 steel as references to identify the properties of a separate unknown material. The calibration phantoms provided information on how accurate the proposed method was expected to be on relatively pure, isotropic and homogenous materials, before the application to human fingernails. It was determined that the 19 MHz ultrasonic probe was capable of obtaining accurate and repeatable results on the calibration phantoms with a maximum percent difference error compared to literature of 17% as found for the zinc phantom. This percent difference may seem high but there are several factors that could have caused this deviation. The ability of the user to maintain the probe tip at an angle directly perpendicular to the material surface was challenging since the polystyrene cone tip had a very small surface area. This made the tip slide on the samples or change angle as the human subject would breathe or move. Also to note is the fact that exact composition of the phantoms and those from the literature may have varied slightly. Although the error compared to literature may be improved, the repeatability of phantom measurements was much more accurate, possibly revealing that there are in fact differences between the molecular composition of the samples used and those in literature. The repeatability of values from the metal phantoms was determined to have a maximum percent difference of 3%, which fell within a 95% confidence interval. The coefficients of variation for all phantoms were low, with a maximum of 1% as seen in aluminum. The probe was then tested on an *in-vivo* fingernail of a 29 year-old male volunteer. The maximum error obtained for the fingernail was 16% which was within the error of the calibration phantoms used. The error could be from the

fingernail thickness or sound speed used which may have been within millimeter distance to where the probe reflection measurements were recorded. Another source of error was that the literature value used was based on an average of fingernail properties from various demographics. The coefficient of variation for the fingernail measurements was much larger than that of the phantoms, as was expected. Only a single fingernail measurement was conducted, and so statistical significance is still to be investigated. Based on these results, the proposed ultrasound reflection method was able to distinguish material parameters to errors below 20% deviation from literature.

Future plans for use of the 19 MHz probe may involve a larger volunteer group of different demographics, as well as further algorithm or probe tip development to accommodate for small angular deviations. Calculation of sound speed is a crucial parameter required for the reflectivity technique, and so a more efficient way determining fingernail thickness and sound speed would be desired. The hardware component may also be reduced in size and connected to a tablet for maximum portability. Based on the prelusive fingernail assessment, it was identified that fingernail changes could be evaluated. Thus, the application of ultrasound to quantitatively assess fingernail properties using reflectance signals validated to be useful in practice. With this in mind, the method could be ideal for clinical applications with further development.

REFERENCES

[1] J. Goulle, E. Saussereau, L. Mahieu, D. Groenwont, S. Lacroix, M. Goullet, C. Guerbet, C. Bouige and C. Goulle, "Application of inductively coupled plasma mass spectrometry multielement analysis in fingernail and toenail as a biomarker of metal exposure," *Journal of Analytical Toxicology,* vol. 22, no. 2, pp. 92-98, 2009.

[2] A. Momen, M. Khalid, M. Elsheikh and A. Dafaalla, "Trace elements in scalp hair and fingernails as biomarkers in clinical studies," *Journal of Health Specialties,* vol. 3, no. 1, p. 28, 2015.

[3] L. Berger, M. Fendrich, J. Jones, D. Fuhrmann, C. Plate and D. Lewis, "Ethyl glucuronide in hair and fingernail as long-term alcohol biomarker," *Addiction,* vol. 109, no. 3, pp. 425-431, 2014.

[4] M. Jones, J. Jones, D. Lewis, C. Plate, M. Fendrich, L. Berger and D. Fuhrmann, "Correlation of the alcohol biomarker ethyl glucuronide in fingernails and hair to reported alcohol consumed," *Alcoholism-clinical and experimental research,* vol. 35, no. 6, p. 16A, 2011.

[5] M. Buzalaf, C. Massaro, M. Rodrigues, R. Fukushima, R. Pessan, G. Whitford and F. Sampaio, "Validation of fingernail flouride concentration as a predictor of risk for dental flourosis," *Caries Research,* vol. 46, no. 4, pp. 394-400, 2012.

[6] R. Fukushima, D. Rigolizzo, L. Maia, F. Lauris, J. Buzalaf, M. Sampaio and M. Buzalaf, "Environmental and individual factors associated with nail flouride concentrations," *Caries Research,* vol. 43, no. 2, pp. 147-154, 2009.

[7] V. Martinez, A. Creus, W. Venegas, A. Arroyo, J. Beck, T. Gebel, J. Surralles and R. Marcos, "Evaluation of micronucleus induction in a chilean population environmentally exposed to arsenic," *Genetic Toxicology and Environmental Mutagenesis,* vol. 564, no. 1, pp. 65-74, 2004.

[8] M. Garland, J. Morris, B. Rosner, K. Stampfer, V. Spate, C. Baskett, W. Willet and D. Hunter, "Toenail trace-element levels as biomarkers- reproducibility over a 6-year period," *Cancer Epidemiology Biomarkers & Prevention,* vol. 2, no. 5, pp. 493-497, 1993.

[9] G. Herman, C. Haver, K. Kozlov, J. Centeno, V. Jurgenson, A. Kolker, K. Conko, E. Landa and H. Xu, "Biomarkers of mercury exposure in two eastern ukraine cities," *Journal of Occupational and Environmental Hygiene,* vol. 8, no. 4, pp. 187-193, 2011.

[10] X. Li, Q. Shi, W. Jin, G. Li, K. Todoroki, H. Muzino, T. Toyo'Oka and J. Min, "Uric acid quantification in fingernails of gout patients and healthy volunteers using HPLC-UV," *Biomedical Chromatography,* vol. 30, no. 8, pp. 1338-1342, 2016.

[11] R. Vacarescu, B. Slak, A. Maeva, C. Hamm, N. Lewoc, A. Daabous, E. Strumban and R. Maev, "Investigation of a correlation between taxane-based chemotherapy and the ultrasonic time-of-flight of human fingernails," *Skin Research & Technology,* pp. 1-6, 2017.

[12] A. Gupta, A. Parakh and A. P. Dubey, "Chemotherapy induced nail changes," *Indian Journal of Dermatology,* vol. 54, no. 4, pp. 204-205, 2008.

[13] G. Hinds and V. D. Thomas, "Malignancy and cancer treatment-related hair and nail changes," *Dermatological Clinics,* vol. 26, pp. 59-68, 2008.

[14] U. Runne and C. Orfanos, "The human nail," *Current Problems in Dermatology,* vol. 9, pp. 102-149, 1981.

[15] A. Y. Finlay, "The physical properties and function of nails," in *The Physical Nature of the Skin*, Lancaster, M.T.P. Press, 1988, p. 143.

[16] S. Yaemsiri, N. Hou, M. Slining and K. He, "Growth rate of human fingernails and toenails in healthy American young adults," *European Academy of Dermatology and Venereology,* vol. 24, pp. 420-423, 2009.

[17] A. Y. Finlay, B. Western and C. Edwards, "Ultrasound velocity in human fingernail

and effects of hydration: validation of in vivo nail thickness measurement techniques," in *British Journal of Dermatology*, vol. 123, 1990, pp. 365-373.

[18] J. Ruan, X. Wang and M. Xia, "The evaluation of nail health conditions with skin ultrasound," *Cutaneous and Ocular Toxicology,* vol. 31, no. 4, pp. 318-322, 2012.

[19] X. Li, G. Li, Y. Jiang, D. Kang, C. Jin, Q. Shi, T. Jin, K. Inoue, K. Todoroki, T. Toyo'Oka and J. Min, "Human nails metabolite analysis: A rapid and simple method for quantification of uric acid in human fingernail by high-performance liquid chromatography with UV-detection," *Journal of Chromotography,* vol. 1002, pp. 394-398, 2015.

[20] W. Wem, Y. Meng, J. Xiao, P. Zhang and H. Zhang, "Comparative study on keratin structural changes in onychomycosis and normal human finger nail specimens by raman spectroscopy," *Journal of Molecular Structure,* vol. 1038, pp. 35-39, 2013.

[21] R. Coopman, T. Van de Vyver, A. Kishabongo, P. KJatchunga, E. Van Aken, J. Cokomola, T. Monteyne, M. Speeckaert and J. Delanghe, "Glycation in human fingernail clippings using ATR-FTIR spectrometry, a new marker for the diagnosis and monitoring of diabetes mellitus," *Clinical Biochemistry,* vol. 50, no. 1-2, pp. 62-67, 2017.

[22] A. Herane-Vives, S. Fischer, V. De Angel and T. Wise, "Cortisol levels in major depressive episode using fingernail specimens," *Psychoneuroendocrinology,* vol. 71, p. 21, 2016.

[23] F. Warnock, K. Mcelwee, R. Seo, S. Mcisaac, D. Seim, T. Ramirez-Aponte, K. Macritchie and A. Young, "Measuring cortisol and DHEA in fingernails: a pilot study," *Neuropsychiatric Disease and Treatment,* vol. 6, pp. 1-7, 2010.

[24] R. H. Hillman, "Fingernail Growth in the Human Subject: Rates and Variations in 300 Individuals," *Human Biology,* vol. 27, no. 4, pp. 274-283, 1955.

[25] D. de Berker, "Nail Anatomy," *Clinics in Dermatology,* vol. 31, pp. 509-515, 2013.

[26] S. Kane, Introduction to physics in modern medicine, Boca Raton: CRC Press, 2009,

pp. 238-249.

[27] A. Briggs, Advances in Acoustic Microscopy, New York: Plenum Press, 1995.

[28] A. Y. Finlay, H. Moseley and T. C. Duggan, "Ultrasound transmission time: an in vivo guide to nail thickness," in *British Journal of Dermatology*, vol. 117, 1987, pp. 765-770.

[29] G. B. E. Jemec and J. Serup, "Ultrasound structure of the human nail plate," *Archives of Dermatology,* vol. 125, pp. 643-646, 1989.

[30] A. R. Maeva, E. Y. Bakulin, L. A. Denisova and R. G. Maev, "Investigation of human nail microstructure with ultrasound," in *Acoustical Imaging*, Windsor, Springer Science, 2008, pp. 199-202.

[31] U. Wollina, M. Berger and K. Karte, "Calculation of nail plate and nail matrix parameters by 20 MHz ultrasound in healthy volunteers and patients with skin disease," Germany, Skin Research and Technology, 2001, pp. 60-64.

[32] T. Hirai and M. Fumiiri, "Ultrasonic observation of the nail matrix," *Elsevier Science Inc.,* vol. 21, pp. 158-161, 1995.

[33] P. R and H. G, "Guidance for Industry and FDA Staff - Information for Manufacturers Seeking Marketing Clearance of Diagnostic Ultrasound Systems and Transducers," 9 9 2008. [Online]. Available: https://www.fda.gov/MedicalDevices/ucm070856.htm. [Accessed 25 10 2017].

[34] P. Hoskins, K. Martin and A. Thrush, Diagnostic ultrasound: physics and equipment, Cambridge University Press, 2010.

[35] W. Hedrick, Technology for diagnostic sonography, Elsevier, 2013.

[36] P. Seutens, Fundamentals of medical imaging, Cambridge: Cambridge University Press, 2009.

[37] A. Ng and J. Swanevelder, "Resolution in Medical Imaging," in *Continuing education in anaesthesia, critical care & pain*, Oxford University press, 2011, pp.

186-192.

[38] R. Feynman, "The Wave Equation," in *Lectures in Physics*, Caltech, 1963.

[39] R. Cobbold, Foundations of Biomedical Ultrasound, Oxford University Press, 2006.

[40] J. Boon, Veterinary echocardiography, John Wiley & Sons, 2011.

[41] P. Laugier and G. Haiat, Introduction to the physics of ultrasound, Dordrecht: Springer, 2011.

[42] P. Laugier and G. Haiat, "Introduction to the physics of ultrasound," in *Bone quantitative ultrasound*, Springer , 2011, pp. 29-45.

[43] N. Hwang and S. Woo, "Frontiers in biomedical engineering," in *Proceedings of the World Congress for Chinese Biomedical Engineers*, Taipei, 2002.

[44] P. White, G. Clement and K. Hynynen, "Longitudinal and shear mode ultrasound propagation in human skull bone," *Ultrasound in medicine and Biology,* vol. 32, no. 7, pp. 1085-1096, 2006.

[45] A. Sarvazyan, A. Skovoroda, S. Emilianov, J. Fowlkes, J. Pipe, R. Adler, R. Buxton and P. Carson, "Biophysical bases of elasticity imaging," *Acoustical Imaging,* vol. 21, pp. 223-240, 1995.

[46] S. Cleator, M. Parton and M. Dowsett, "The biology of neoadjuvent chemotherapy for breast cancer," *Society for Endocrinology,* vol. 9, pp. 183-195, 2002.

[47] P. Gilbar, A. Hain and V.-M. Peereboom, "Nail toxicity induced by cancer chemotherapy," *Journal of Oncology Pharmacy Practice,* vol. 15, pp. 143-155, 2009.

[48] R. Fawcett, S. Linford and Stulberg DL, "Nail abnormalities: clues to systemic disease," *American Family Physician,* pp. 1417-1424, 2004.

[49] E. Ghetti, B. Piraccini and A. Tosti, "Onycholysis and subungual haemorrhages secondary to systemic chemotherapy (paclitaxel)," *European Academy of Dermatology and Venerology,* vol. 17, pp. 459-460, 2003.

[50] C. Robert, V. Sibaud, M. Christina, Verschoore, C. Michele, E. Lanoy and R. Baran, "Nail toxicities induced by systemic anticancer treatments," vol. 16, no. 4, 2015.

[51] S. M. Ricci and W.-X. Zong, "Chemotherapeutic approaches for targetting cell death," *National Institute of Health,* vol. 11, no. 4, pp. 342-357, 2006.

[52] M. D. Stubblefield and M. O'Dell, "Principles of chemotherapy," in *Synopsis of Clinical Oncology*, New York, Demos Medical Publishing, 2010, pp. 15-45.

[53] R. T. Skeel and S. N. Khleif, Handbook of cancer chemotherapy, Philadelphia: Lippincott Williams & Wilkins, 2011, pp. 330, 427, 698, 744, 761, 783, 830.

[54] L. Paul J and P. Cohen R, "Pacliataxel-associated subungual pyogenic granuloma: report in a patient with breast cancer recieving paclitaxel and review of drug-induced pyogenic granulomas adjacent to and beneath the nail," *Journal of Drugs in Dermatology,* vol. 11, no. 2, pp. 262-268, 2012.

[55] B. Piraccini and M. Iorizzo, "Drug reactions affecting the nail unit: diagnosis and management," *Dermatologic Clinics,* pp. 215-219, 2007.

[56] A. M. Minisini, A. Tosti, A. F. Sobrero, M. Mansutti, B. M. Piraccini, C. Sacco and F. Puglisi, "Taxane-induced nail changes: incidence, clinical presentation and outcome," *Annals of Oncology,* vol. 14, no. 2, pp. 333-337, 2003.

[57] T. Postma and J. Heimans, "Grading of chemotherapy-induced peripheral neuropathy," *Annals of Oncology,* vol. 2, pp. 509-513, 2000.

[58] K. Kibata, T. Tamaki, N. Inagaki, M. Ogata, T. Shimizu and S. Nomura, "Nail alterations as a surrogate marker for the efficacy of low-dose metronomic chemotherapy," *Oncology Letters,* vol. 5, p. 1127, 2013.

[59] L. Farran, A. Ennos, M. Starkie and S. Eichhorn, "Tensile and shear properties of fingernails as a function of a changing humidity environment," vol. 42, 2009.

[60] J. Blitz and G. Simpson, "Reflection and transmission at normal incidence," in *Ultrasonic methods of non-destructive testing*, London, Champman & Hall, 1996, pp. 19-27.

[61] S. Hoche and M. B. T. Hussein, "Density, ultrasound velocity, acoustic impedance, reflection and absorption coefficient determination of liquids via multiple reflection method," *Ultrasonics,* vol. 57, pp. 65-71, 2015.

[62] R. Higuti and J. Adamowski, "Ultrasonic densiometer using a multiple reflection technique," *IEEE Transactions,* vol. 49, no. 9, pp. 1260-1268, 2002.

[63] C. Chung, J. Popovics and L. Struble, "Using ultrasonic wave reflection to measure solution properties," *Ultrasonics Sonochemistry,* vol. 17, pp. 266-272, 2010.

[64] W. Drexler and J. Fujimoto, Optical coherence tomography: technology and applications, Springer, 2008.

[65] V. Hanel and B. Kleffner, "Double focus technique for simultaneous measurement of sound velocity and thickness of thin samples using time-resolved acoustic microscopy," *Acoustical Imaging,* vol. 24, pp. 187-191, 2000.

[66] A. Wydra, E. Malyarenko, K. Shapoori and M. RG, "Development of a practical ultrasonic approach for simultaneous measurement of the thickness and the sound speed in human skull bones: a laboratory phantom study," *Physics in Medicine and Biology,* vol. 58, pp. 1083-1102, 2013.

[67] A. Baraldi, S. Jones, S. Guesne, M. Traynor, W. McAuley, M. Brown and S. Murdan, "Human nail plate modifications induced by onychomycosis: implications for topical therapy," *Pharmaceutical Research,* vol. 32, pp. 1626-1633, 2015.

[68] H. Baden, "The physical properties of nail," *The Journal of Investigative Dermatology,* vol. 55, no. 2, pp. 115-122, 1970.

[69] D. Ensminger, Ultrasonics, New York: Marcel Dekker, 1988.

[70] S. Flory, D. Solimando Jr, G. Webster, C. Dunton, J. Neufeld and M. Haffey, "Onycholysis associated with weekly administration of paclitaxel," *The Annals of Pharmacology,* vol. 33, pp. 584-586, 1999.

[71] S. Hussain, N. Anderson, M. Salvatti, B. Adamson, M. McManus and A. Braverman, "Onycholysis as a complication of systemic chemotherapy," *Cancer,*

vol. 88, no. 10, pp. 2367-2371, 2000.

[72] L. Paul and P. Cohen, "Paclitaxel-associated subungual pyogenic granuloma: report in a patient with breast cancer recieving paclitaxel and review of drug-induced pyogenic granulomas adjacent to and beneath the nail," *Journal of Drugs in Dermatology,* vol. 11, no. 2, pp. 262-268, 2012.

VITA AUCTORIS

Rares Anthony Vacarescu was born in Sibiu, Romania in the year 1992. He graduated from St. Joseph's High School in 2010. From there he went on to complete an Honors Bachelor degree in Medical Physics (with Thesis and Coop) at the University of Windsor in 2015. He is currently a candidate for a Masters in Physics at the University of Windsor and plans to graduate in Fall 2017.